The [(NH3)4Cu2O2]2+-Peroxo Complex as the Key Intermediate for NH3-SCR Activity and Deactivation of Cu-CHA Catalysts

ChemCatChem

Review
doi.org/10.1002/cctc.202400384

Chemistry Europe
European Chemical Societies Publishing

www.chemcatchem.org

The $[(NH_3)_4Cu_2O_2]^{2+}$-Peroxo Complex as the Key Intermediate for NH_3-SCR Activity and Deactivation of Cu-CHA Catalysts.

Ton V.W. Janssens,[a] Elisa Borfecchia,[b] Kirill A. Lomachenko,[c] Henrik Grönbeck,[d] and Gloria Berlier[b]

In NH_3-SCR over Cu-CHA catalysts in the low-temperature range 150–300 °C, the activation of oxygen occurs via oxidation of a pair of mobile $(NH_3)_2Cu^I$-complexes located in the cages of the zeolite. In this step, a reactive $[(NH_3)_4Cu_2O_2]^{2+}$-peroxo complex (μ-η^2,η^2-peroxo diamino dicopper(II)-complex) is formed. The chemistry of this complex determines several catalytic properties of the Cu-CHA catalyst. The reaction of NO with the $[(NH_3)_4Cu_2O_2]^{2+}$-peroxo complex governs the NH_3-SCR activity. A reaction of the $[(NH_3)_4Cu_2O_2]^{2+}$-peroxo complex with ammonia hinders the reaction of NO with the complex, thus leading to an inhibition of the NH_3-SCR reaction. Finally, the deactivation in presence of SO_2 is due to a reaction of SO_2 with the $[(NH_3)_4Cu_2O_2]^{2+}$-peroxo complex, leading to the formation of Cu–S compounds in the catalyst. In this review, the characterization and the reactions of the $[(NH_3)_4Cu_2O_2]^{2+}$-peroxo complex with NO, NH_3, and SO_2, and mean-field kinetic models based on first principles calculations for NH_3-SCR activity and SO_2 poisoning are discussed.

1. Introduction

Since the discovery of Cu-chabazite materials (Cu-CHA, also referred to as Cu-SSZ-13) as effective catalysts for selective catalytic reduction by ammonia (NH_3-SCR),[1–3] these have become a widely applied catalyst for the abatement of NOx in diesel-powered passenger cars and heavy-duty vehicles. In the NH_3-SCR reaction, NOx is reduced to nitrogen and water by ammonia, which is added to the exhaust gas via injection of a urea solution (AdBlue® or Diesel Exhaust Fluid (DEF)). Cu-CHA catalysts feature excellent NH_3-SCR activity at temperatures in the 150–300 °C range, and a good thermal stability. This means that they generally can be operated in the temperature window 150–550 °C, as is required for application in exhaust systems. The thermal stability of Cu-CHA catalysts ensures that the Cu-CHA catalysts can be exposed to temperatures up to about 800 °C, without significant degradation of the zeolite material.[4,5] This makes these catalysts very robust in the harsh and dynamic environment in exhaust systems. Another attractive property of Cu-CHA catalysts for NH_3-SCR is that such catalysts have a low selectivity for N_2O formation, as compared to other Cu-zeolite systems.[5,6] Because N_2O is a strong greenhouse gas with a global warming potential of about 300,[7] the use of Cu-CHA catalysts also contributes to minimize greenhouse gas emissions from exhaust systems.

In the NH_3-SCR reaction, the conversion of NOx – which in this article refers to the NO and NO_2 compounds combined – to N_2 and H_2O by NH_3 takes place according to the standard-SCR reaction, which follows the equation: (Eq 1):

$$4\ NO + 4\ NH_3 + O_2 \rightarrow 4\ N_2 + 6\ H_2O \quad (1)$$

When NO_2 is present, the reaction is accelerated, and proceeds according to the fast-SCR reaction:

$$2\ NO + 4\ NH_3 + 2\ NO_2 \rightarrow 4\ N_2 + 6\ H_2O \quad (2)$$

In situations where the concentration of NO_2 exceeds the NO concentration, the NO_2-SCR reactions also contribute to the conversion of NOx:[8]

$$2\ NO_2 + 4\ NH_3 + O_2 \rightarrow 3\ N_2 + 6\ H_2O \quad (3)$$

$$2\ NO_2 + 2\ NH_3 \rightarrow NH_4NO_3 + N_2 + H_2O \quad (4)$$

$$6\ NO_2 + 8\ NH_3 \rightarrow 7\ N_2 + 12\ H_2O \quad (5)$$

As illustrated by the equations above, the NO_2-SCR reactions, taking place in the absence of NO, describe a more complex reaction scheme. Because the exhaust gas of fuel-lean combustion engines, such as diesel engines, typically contains 5–10% oxygen, together with a NO_2/NO ratio lower than 1, the standard-SCR (Eq. 1) and fast-SCR (Eq. 2) reactions are the most

[a] T. V.W. Janssens
Umicore Denmark ApS, Kogle Allé 1, 2970 Hørsholm, Denmark
[b] E. Borfecchia, G. Berlier
Department of Chemistry and NIS Centre, University of Turin, via Giuria 7, 10125 Turin, Italy
[c] K. A. Lomachenko
European Synchrotron Radiation Facility, 71 avenue des Martyrs, CS 40220, 38043 Grenoble Cedex 9, France
[d] H. Grönbeck
Department of Physics and Competence Centre for Catalysis, Chalmers University of Technology, SE412 96 Göteborg, Sweden

relevant reactions for the abatement of NOx in diesel exhaust systems. Here, we focus exclusively on the standard-SCR reaction, and, in particular, the mechanism of that reaction in the 150–300 °C temperature range.

As the reaction products in the standard-SCR reaction do not contain an O—O bond (Eq. 1), the NH_3-SCR reaction implies a dissociation of the O—O bond in the O_2 molecule. In Cu-CHA catalysts, the dissociation of the O_2 molecule involves the formation of a μ-η^2,η^2-peroxo diamino dicopper(II) ($[(NH_3)_4Cu_2O_2]^{2+}$-peroxo) complex. This $[(NH_3)_4Cu_2O_2]^{2+}$-peroxo complex is key for the NH_3-SCR activity over Cu-CHA catalysts,[9,10] but, at the same time, it is also an important channel for deactivation by SO_2. The NH_3-SCR activity is related to the reactivity of this complex towards NO and NH_3; the dissociation of the O_2 molecule then takes place in the reactions of the $[(NH_3)_4Cu_2O_2]^{2+}$-peroxo complex with these molecules. The deactivation of Cu-CHA catalysts by SO_2 is a consequence of the reactivity of the $[(NH_3)_4Cu_2O_2]^{2+}$-peroxo complex with SO_2.[11–13] These aspects illustrate how the chemistry of the $[(NH_3)_4Cu_2O_2]^{2+}$-peroxo complex is pivotal for the fundamental understanding of Cu-CHA catalysts for NH_3-SCR. In this review, we discuss the identification of the $[(NH_3)_4Cu_2O_2]^{2+}$-peroxo complex as a reaction intermediate in the standard-SCR reaction (Eq. 1), and how its chemistry determines the kinetics of that reaction, the formation of N_2O, and deactivation by SO_2.

2. Importance of Mobility and Cu-Pair Formation for Activation of O_2

In the NH_3-SCR reaction cycle, the Cu ions in the zeolite undergo alternating oxidation and reduction steps, whereby the oxidation state changes between Cu^{I} and Cu^{II}. In fact, the oxidation and reduction steps have been executed separately.[14–21] For the oxidation half-cycle, the catalyst is exposed to O_2 or a mixture of O_2 and NOx; the reduction takes place in a mixture of NO and NH_3 in the absence of O_2. Because

Ton V.W. Janssens is Senior Scientist at Umicore Denmark ApS in the Automotive Catalysis department, working on catalysts for the selective catalytic reduction of NOx diesel exhaust systems. Ton obtained his PhD in 1993 at the Eindhoven University of Technology, the Netherlands, in the field of surface science. He then moved to the University of California, Riverside, and the Fritz-Haber Institute, Berlin, as a postdoc, after which he joined Topsoe (Denmark) in 1998. At Topsoe he initially worked on catalysts for syngas conversion, and zeolite catalysis. He moved to the Automotive Catalysis department in 2012, and joined Umicore in 2017.

Elisa Borfecchia obtained her PhD degree in 2013 at the University of Turin. During her PhD and afterward, her research centred on characterizing functional materials by X-ray spectroscopy. From 2016, she worked at Haldor Topsøe A/S and she was subsequently awarded a Marie Curie Fellowship to join the Catalysis group at Oslo University. From 2019, she has been assistant professor in Physical Chemistry at the University of Turin, where she is currently Associate Professor. She authored >90 peer-reviewed papers and performed >60 experiments at synchrotrons, aimed at disclosing local structure and reactivity of metal centres in heterogeneous catalysts.

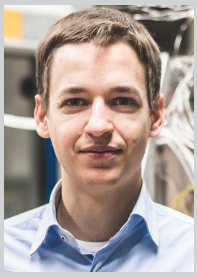

Kirill A. Lomachenko is responsible for the chemistry research programme at BM23 and ID24 XAS beamlines of the European Synchrotron Radiation Facility (France). He completed his PhD under the joint supervision of Profs. Carlo Lamberti (University of Turin, Italy) and Alexander Soldatov (Southern Federal University, Russia) in the intersection of physics, chemistry, and materials science. His main field of research is the application of XAS and XES spectroscopies and related characterization techniques to establish the structure-property relationships of novel materials for catalysis, energy storage, and gas sorption.

Henrik Grönbeck received his PhD in Physics from Göteborg University in 1996 with a thesis on electronic and structural properties of metal clusters. He joined Chalmers in 2001 after working at Ericsson Microwave Systems and a postdoc position at IBM Research Zurich. Grönbeck was promoted to professor in 2012 and is presently the head of the Division of Chemical Physics. His group is working within computational catalysis and surface science, and one main research direction is to develop kinetic models based on density functional theory calculations.

Gloria Berlier received her PhD in Chemical Science from the University of Turin in 2001 with a thesis on the structure and reactivity of iron clusters in zeolites. She worked as postdoc at the DFRL of the Royal Institution of GB in London and at the Department of Chemistry of University of Turin. Since 2021 she is Full Professor in Physical Chemistry. She works at the characterization of heterogeneous catalysts, focusing on the structure and reactivity of surface sites. Her experimental approach involves in situ and operando optical spectroscopies, electronic microscopy, gas-volumetric and structural techniques.

O_2 does not react with any of the Cu^{II} species in the NH_3-SCR reaction cycle, the activation of O_2 implies an oxidation of Cu^{I}.[9,14,15,17,18,22] Moreover, this is the only possible reaction step to oxidize the Cu^{I} to Cu^{II} in the standard-SCR reaction cycle, as neither NO nor NH_3 undergo a reaction with Cu^{I}. This strict selectivity of the reactivity of O_2 to Cu^{I} is the reason why the oxidation and reduction half-cycles in the NH_3-SCR reaction can be done separately.[14–16,23–27]

The reaction of an O_2 molecule with Cu^{I} is not a straightforward elementary step, as follows from the stoichiometry of the NH_3-SCR reaction. According to Eq. 1, a single O_2 molecule reacts with four molecules of NO and NH_3, to form H_2O and nitrogen. That process requires the transfer of four electrons to the oxygen from the other reactants. Since a single Cu^{I} ion can only transfer one electron, it follows that the reaction of O_2 requires either a reaction of a single O_2 molecule with four Cu ions in the zeolite, or the participation of an alternative electron donor. The formation of the $[(NH_3)_4Cu_2O_2]^{2+}$-peroxo complex suggests, that the actual NH_3-SCR reaction cycle involves a reaction of an O_2 molecule with two Cu ions, accounting for the transfer of two electrons. The remaining two electrons are eventually delivered by the NO reactant. An early indication that two Cu ions are required in the NH_3-SCR reaction follows from the observation that the catalytic activity of Cu-CHA catalysts show a 2nd order dependence on the Cu content.[26,28–32]

Density functional theory (DFT) calculations indicate, that the activation of an O_2 molecule becomes significantly easier when it can interact with two Cu ions simultaneously, resulting in formation of binuclear or multinuclear Cu_xO_y species.[33,34] Reactions with O_2 and two Cu^{I} ions bound to the zeolite framework are possible, but generally they require suitable configurations of the Cu ions, dictated by the crystal structure and Si/Al ratio of the zeolite.[35] This means that stabilization of Cu_xO_y species requires certain framework structural motifs. As an example, a mono(μ-oxo)dicopper core in ZSM-5 should be located at the intersection of straight and sinusoidal ten-membered rings, formed by O_2 (or N_2O) reaction with two Cu^{I} ions at distance of 4.17 Å.[36,37] A similar structure can be formed in Cu-mordenite at a different structural motif, *i.e.* at the intersection of the side pocket with the 12 and 8 member rings channels, with an adjacent Al framework atoms distance around 7.55 Å.[38] In Cu-CHA, O_2 can be activated by two Cu^{I} ions, when both ions are located in an 8-membered ring.[39]

With Cu-ions fixed to the zeolite crystal, and a random distribution of the possible Cu-exchange sites generated by the Al atoms in the zeolite framework, the number of possible sites with two Cu-ions that can "fit" a single O_2 molecule is limited. If the Cu ions become mobile, it is easier to form suitable Cu-pairs. Some mobility of Cu ions has been observed during thermal treatment of the catalyst,[40–43] where Cu^{I} ions formed by 'self-reduction' of Cu^{II} during heating in inert gas migrate from an 8-membered ring to the double-6-rings typical of the CHA structure.[42] Similarly, a redistribution of Cu^{II} ions initially present as Z-Cu^{II}OH in 8-membered rings (Z represents a negative charge on the zeolite framework) to Z_2-Cu^{II} in the 6-membered rings has been observed during thermal treatment in air.[43]

In Cu-CHA based catalysts, the Cu ions are coordinated by NH_3, NO_3^-, NO_2^-, and OH^- ligands under conditions for NH_3-SCR below 300 °C, forming Cu-complexes.[14,15,17,18,44] In particular, the Cu^{I} species is a linear $(NH_3)_2Cu^{I}$ complex, which can be identified by a characteristic pre-edge peak at the Cu–K edge in the X-ray absorption (XAS) spectrum.[15,17,45,46] The absence of a clear Cu–Si or Cu–Al coordination in the Extended X-ray Absorption Fine Structure (EXAFS) after the formation of this complex indicates a weak interaction of the $(NH_3)_2Cu^{I}$ complex with the zeolite framework.[15,17,47] Ab-initio molecular dynamics calculations show that this weak interaction allows for some mobility of the complex in the zeolite cages.[17,47–49] Furthermore, gas phase NH_3 induces a solid-state ion exchange process in a physical mixture of CuO or Cu_2O and a H-CHA zeolite at temperatures as low as 250 °C, under the formation of the $(NH_3)_2Cu^{I}$ complex.[48,50–52] This observation provides experimental evidence for an enhanced mobility of the $(NH_3)_2Cu^{I}$ complex under SCR conditions.

In the NH_3-SCR reaction over Cu-CHA catalysts via Cu-pair formation, the mobility of the $(NH_3)_2Cu^{I}$ complexes facilitates the activation of O_2.[18,30,34,47] As a consequence, the oxidation step of the linear $(NH_3)_2Cu^{I}$ complexes by O_2 shows a 2nd order dependence on the Cu-content of the catalyst.[16,30,32] When the Cu content in the catalyst decreases, an increasing fraction of the $(NH_3)_2Cu^{I}$ complexes does not react with O_2, and remains in the reduced state.[30,53] Calculations of the molecular dynamics of the system indicate that the $(NH_3)_2Cu^{I}$ complexes can move up to about 9 Å away from their anchor point in the zeolite.[17,30] At lower Cu loadings, the average distance between two Cu ions becomes larger, and therefore the propensity of suitable $(NH_3)_2Cu^{I}$ pairs for O_2 activation decreases in catalysts with low Cu content, resulting in the observed 2nd order behavior. In transient kinetic models, this 2nd order behavior has been explicitly implemented, to produce accurate descriptions of the individual oxidation and reduction steps in the NH_3-SCR cycle.[16,20,22,26,27,32]

Direct experimental evidence for importance of the mobility of $(NH_3)_2Cu^{I}$ complexes for the oxidation step in the NH_3-SCR reaction cycle is provided by a calorimetry study of the reactivity of framework-bound Cu^{I} and $(NH_3)_2Cu^{I}$, showing a stronger reaction of oxygen with the $(NH_3)_2Cu^{I}$ complexes.[54] Figure 1 shows that, at temperatures below 200 °C, the heat release upon reaction of oxygen with $(NH_3)_2Cu^{I}$ complexes (2 to 3 J/g_{cat}) is clearly higher compared to framework Cu^{I}. These results indicate that the presence of $(NH_3)_2Cu^{I}$ complexes enhances the reaction with O_2, in line with the idea that the mobile $(NH_3)_2Cu^{I}$ complexes facilitate the Cu-pair formation that is needed for the reaction with oxygen. The increase in heat release with the reaction temperature indicate that the reactions of oxygen with the $(NH_3)_2Cu^{I}$ complexes and framework Cu^{I} species are activated processes, with estimated activation energies of 15 kJ/mol and 39 kJ/mol,[54] respectively. The decrease in heat release for the $(NH_3)_2Cu^{I}$ complexes above 200 °C correlates well with the temperature range where the decomposition of the $(NH_3)_2Cu^{I}$ complexes takes place,[55–57]

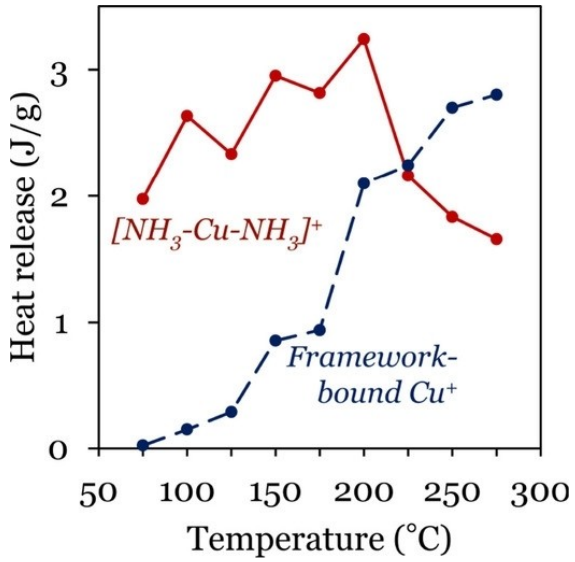

Figure 1. Heat release upon exposure to 500 ppm O_2 at various temperatures between 75 and 275 °C over the $(NH_3)_2Cu^I$ complexes (red dots/solid line) and the framework-bound Cu^I species (blue dots/dashed line) in 3 wt% Cu-CHA catalyst. Reprinted with permission from Ref. [54]. Copyright © 2021 X. Wang et al. ChemCatChem published by Wiley-VCH GmbH.

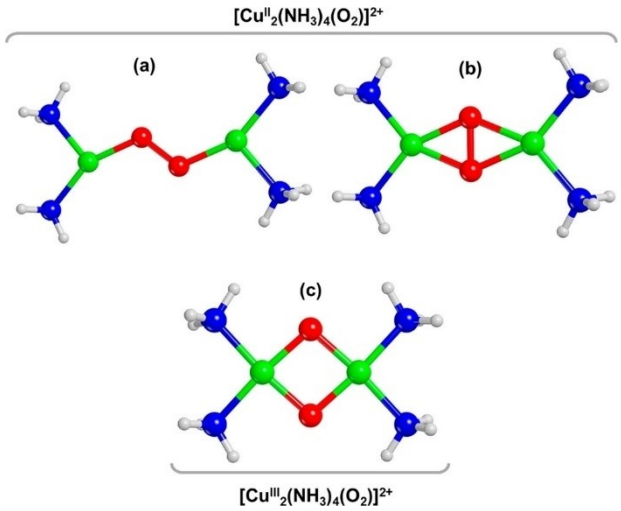

Figure 2. Ball-and-stick drawings of the three most probable $[Cu_2(NH_3)_4O_2]^{2+}$ complexes: (a) trans-μ-1,2-peroxo diamino dicopper(II) (end-on), (b) μ-η^2,η^2-peroxo diamino dicopper(II) (side-on), and c) bis-μ-oxo diamino dicopper(III). Atom color code: Cu, green; H, white; O, red; N, blue. Reproduced from Ref. [24]. Copyright © 2020 American Chemical Society. Publication licensed under CC-BY 4.0.

leading to a slower oxidation reaction, as the Cu loses its mobility. The oxidation of the framework-bound Cu^I species becomes more prominent above 200 °C, suggesting that the oxidation of framework-bound Cu^I potentially plays a role in the NH_3-SCR reaction at higher temperatures.[18,39,58] Such a change in reaction mechanism explains the often observed decrease in NOx conversion between 300 and 400 °C ("seagull" effect).[39]

Finally, the results shown in Figure 1 provide an efficient experimental procedure to prepare the $[(NH_3)_4Cu_2O_2]^{2+}$-peroxo complex in a Cu-CHA catalyst. First, the $(NH_3)_2Cu^I$ complex is formed by reduction of the catalyst at 200–250 °C, to ensure complete reduction. In a second step, the catalyst is exposed to at least 4% O_2 at 200 °C,[54] in order to form the $[(NH_3)_4Cu_2O_2]^{2+}$-peroxo complex. This procedure is of great value in experimental studies of the chemistry of the $[(NH_3)_4Cu_2O_2]^{2+}$-peroxo complex.

3. Identification of the $[(NH_3)_4Cu_2O_2]^{2+}$-Peroxo Complex

The most probable products of a reaction of O_2 with a pair of $(NH_3)_2Cu^I$ complexes ions are (1) a trans-μ-1,2-peroxo diamino dicopper(II) complex, with an end-on orientation of the O_2 molecule between the Cu-ions, (b) a μ-η^2,η^2-peroxo diamino dicopper(II) complex (the $[(NH_3)_4Cu_2O_2]^{2+}$-peroxo complex), with a side-on orientation of the O_2 molecule, without a complete dissociation of the O_2 bond, or (c) bis-μ-oxo diamino dicopper(III)- complex, a side-on orientation of the O_2 molecule, combined with a O–O bond dissociation. These structures are shown in Figure 2. Based on DFT calculations, EXAFS and UV-Vis spectroscopy, it has been shown that the μ-η^2,η^2-peroxo diamino dicopper(II) complex is formed in the reaction of the linear $(NH_3)_2Cu^I$ complexes with O_2.[24,59,60]

The density functional theory (DFT) has become the standard approach to calculate reaction energies in heterogeneous catalysis, as it generally combines computational efficiency with reasonable accuracy.[61] However, the problem to determine the structure of the reaction product formed in the oxidation of a pair of $(NH_3)_2Cu^I$ complexes with DFT is that the result critically depends on the choice of the exchange-correlation functional. This is illustrated in Figure 3, which shows calculated reaction paths for the reaction of a pair of $(NH_3)_2Cu^I$ complexes with O_2, for different choices of the functional.[59] The oxygen dissociation path is divided in steps with five structures denoted C1 to C5. In general, all functionals indicate that Cu-pairs are favorable for oxygen adsorption. Some of the functionals based on the Perdew-Burke-Ernzerhof (PBE) formula[62] predict the formation of a bis-μ-oxo diamino dicopper(III) complex (Figure 3 C5/Figure 2c). In contrast, the Bayesian error estimation functional (BEEF), PBE functionals augmented with a Hubbard-U term (PBE+U), and PBE+U functionals with corrections to account for Van der Waals interactions (PBE+U+D2) and (PBE+U+D3), and finally a hybrid functional HSE06, all point to the formation of a μ-η^2,η^2-peroxo diamino dicopper(II) complex (Figure 3 C4/Figure 2b). Based on calculations of similar Cu,O-complex structures in enzymes with experimentally verified structures, it could be shown that the PBE+U+D3 approach is a reasonable compromise between computational efficiency and accuracy.[59] Using this functional, with U = 6 eV for the Hubbard term,[59] we find that the oxidation of a pair of $(NH_3)_2Cu^I$ complexes with oxygen results in the side-on configuration, forming a μ-η^2,η^2-peroxo diamino dicopper(II) complex (Figure 3 C4/Figure 2b).

The fact that the results depend on the choice of functional illustrates that DFT methods based on the Generalized Gradient

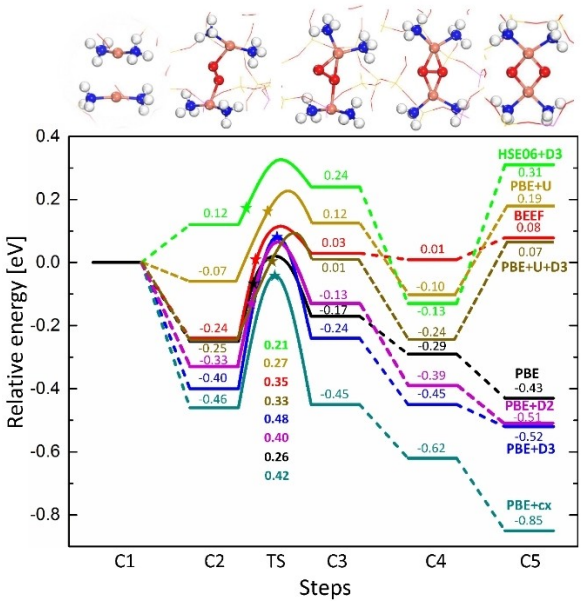

Figure 3. Potential energy landscapes for oxidation of $(NH_3)_2Cu^I$-pairs in CHA calculated by different functionals. The structures considered in each step are shown in the top. TS stands for the transition state from C2 to C3, which include a triplet to singlet transition. The barriers are listed below the curves with the corresponding colors. The stars in the potential energy landscape represent the cross-over between triplet and singlet state for O_2 adsorbed on the pair. All energies are zero-point energy corrected. Atom color codes: copper (pink), aluminum (purple), nitrogen (blue), silicon (yellow), oxygen (red) and hydrogen (white). Reproduced from Ref. [59], with permission from the PCCP Owner Societies.

Approximation (GGA) are not sufficient to describe the system. The main reason is the poor description of charge transfer processes due to the self-interaction error, thus incomplete cancellation of the electron self-interaction between the direct Coulomb interaction and the exchange correlation functional. Moreover, GGA functionals do not account for the van der Waals interactions. Because the $[Cu_2O_2(NH_3)_4]^{2+}$ peroxo complex in CHA is floating in the van der Waals interactions and Coulomb interactions from the zeolite framework, a functional accounting for these interaction is required. The van der Waals interactions can be accounted for by semi-empirical methods, corresponding to the D2 and D3 functionals, or through a proper nonlocal correlation term in the exchange-correlation functional (vdW-DF),[63–66] which was used in the results denoted CX,[67] or the BEEF functional.[68]

The preference for the side-on or bis-configuration is largely determined by the way the degree of electron delocalization is calculated. The functionals with large electron delocalization yield the bis-μ-oxo diamino dicopper(III), while the functionals where the delocalization is suppressed favor the μ-η^2,η^2-peroxo diamino dicopper(II) side-on configuration. The Hubbard-U term controls the electron localization for the PBE functionals, and in the HSE06 hybrid functional, the electron localization is favored by including a part of Fock-exchange. Apparently, the PBE+U–D3 functional results in an adequate description of the Van der Waals interactions and electron delocalization for the Cu–O interactions in Cu-CHA materials.

Whether a bis-μ-oxo diamino dicopper(III) or a μ-η^2,η^2-peroxo diamino dicopper(II) complex is formed upon oxidation of a pair of Cu^I depends on the ligands that are attached to the Cu ions.[59,69] In principle, the two complexes form an equilibrium, which can be shifted by changing the ligands and environment of the Cu–O cores.[69] In fact, a transition state energy of 0.16 eV was calculated for this transition in a Cu-CHA, using a - less appropriate - BEEF-vdW functional.[34] With the NH_3-ligands, the μ-η^2,η^2-peroxo diamino dicopper(II) is clearly favored in Cu-CHA catalysts, which is further confirmed by spectroscopy, as shown below.

Experimental evidence for the formation of a μ-η^2,η2-peroxo diamino dicopper(II) complex, as derived from DFT, comes primarily from in-situ X-ray absorption spectroscopy (XAS) and DR-UV-vis spectroscopy.[24] The X-Ray Near Edge spectra (XANES) of a reduced Cu-CHA catalyst (Si/Al = 15; Cu/Al = 0.5, corresponding to a Cu density of ~0.4 Cu/1000 Å^3) shows that most (84 ± 8 %) of the Cu^I is oxidized to Cu^{II} when exposed to O_2 at 200 °C, in good agreement with the mechanism based oxygen activation on mobile $(NH_3)_2Cu^I$ complexes.[30] The Cu^{II} species formed upon exposure to O_2 at 200 °C shows distinct XANES, EXAFS and DR-UV-Vis spectroscopic features (red curves in Figure 4a-c), that are different from those observed after pretreatment in O_2 at 400 °C (grey dashed curves in Figure 4a-c). Because the latter are due to monomeric and multimeric Cu^{II} species coordinated to the zeolite framework,[70,71] this indicates that the oxidation with O_2 at 200 °C of $(NH_3)_2Cu^I$ complexes leads to a different Cu species.

A Wavelet Transform (WT) analysis of the EXAFS data yields a first indication for the formation of a Cu-complex with two Cu centers. This analysis is based on a 2D representation of the EXAFS data, showing the dependence in both R-space and *k*-space. In particular, the k-space dependency allows for a discrimination of the scattering contributions involving a Cu-atom from those that exclusively involve the lighter elements, such as O/N or Al/Si, due to element-specific k-space dependency of the EXAFS back-scattering amplitude functions F(k) (Figure 4f, top panel). In particular, a sub-lobe centered around k = 7 Å^{-1} is diagnostic for a Cu–Cu scattering path. Figure 4e and f show a clear increase in this Cu–Cu scattering upon oxidation of the linear $(NH_3)_2Cu^I$ complexes by oxygen at 200 °C, indicating the formation of a complex with two Cu centers. The calculated EXAFS scattering for the three structure models shown in Figure 2 indicate that the measured data are most consistent with the expected EXAFS for the μ-η^2,η^2-peroxo diamino dicopper (II) complex, with a Cu–Cu distance of ~3.40 Å.

In DR-UV-Vis spectra, the formation of the μ-η^2,η^2-peroxo diamino dicopper (II) complex is indicated by a broad band in the d-d region centered at 13850 cm^{-1} (~720 nm) and a red-shift of the LMCT transitions (ligand-to-metal charge transfer), that differs from that associated with the framework-coordinated Cu^{II} species in the pre-treated Cu-CHA catalyst (Figure 4c).[24] Upon exposure of Cu-CHA and Cu-AEI catalysts to an NH_3-SCR feed at 250 °C, a distinct band in the 370–350 nm range of the DR-UV-Vis spectrum becomes most prominent. With the aid of DFT calculations and comparison to bio-

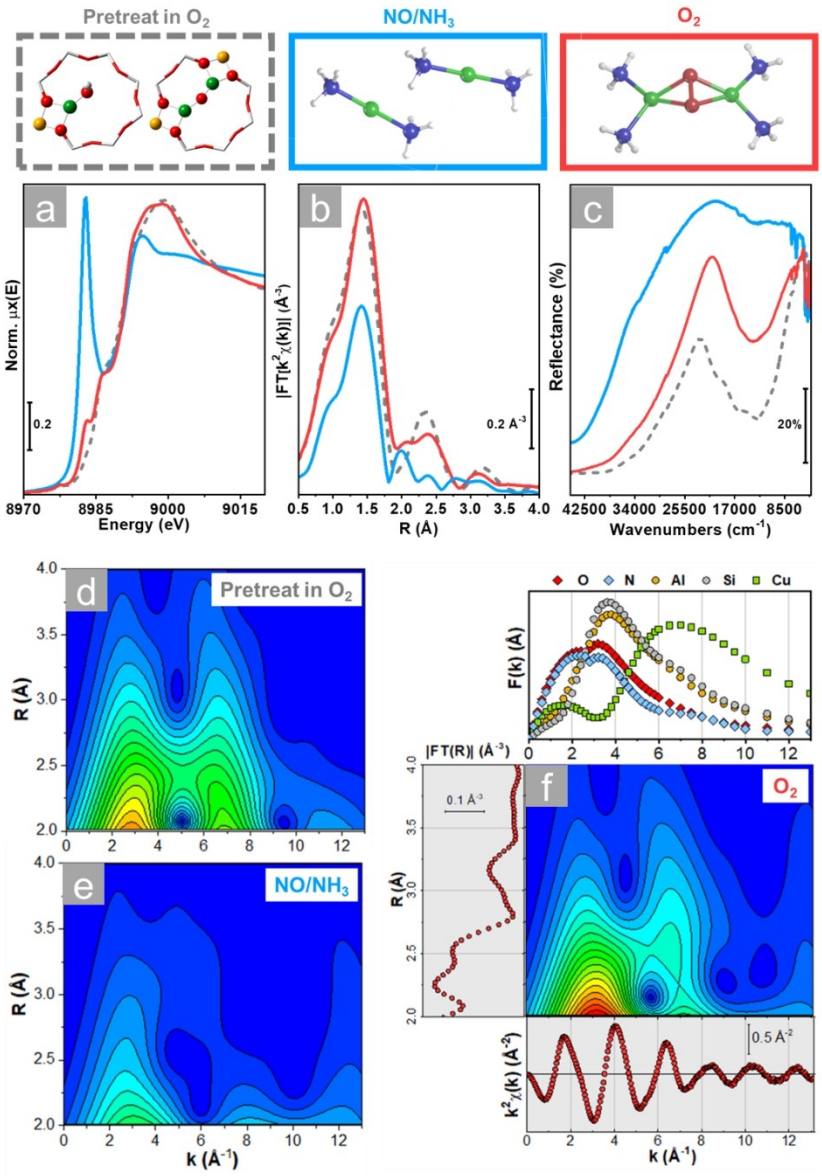

Figure 4. a) XANES, (b) EXAFS and (c) UV-Vis spectra of Cu-CHA (Si(Al = 15, Cu/Al = 0.5) after pretreatment in O_2 (grey dashed curve), reduction in NO/NH_3 (blue) and subsequent reaction with O_2 (red) at 200 °C. The top panel reports a pictorial representation of the dominant Cu-species expected at each step, using the same color code. Atom color code in the structures: Cu, green; H, white; O, red; N, blue, Al, yellow; Si, grey. (d–f) Moduli of EXAFS WTs in the 2–4 Å R-space range for (d) pre-treatment in O_2, (e) reduction in NO/NH_3, (f) subsequent reaction with O_2; part (f) also includes the corresponding EXAFS spectra in k- and R-space (conventional FT), as well as the backscattering amplitude function F(k) of relevant atoms. Summary of results presented in Ref. [24].

inorganic cores,[72] this band can be assigned to the μ-η²,η²-peroxo diamino dicopper (II) complex,[60] further corroborating the role of this species as a key intermediate in the SCR cycle.

4. Structure of the $[(NH_3)_4Cu_2O_2]^{2+}$-Peroxo Complex

Because the $[Cu_2O_2(NH_3)_4]^{2+}$ peroxo complex is formed in a reaction between mobile $(NH_3)_2Cu^{I}$ complexes and O_2, and the mobility of the $(NH_3)_2Cu^{I}$ complexes is affected by the density and distribution of the Al atoms in the zeolite framework, it is reasonable to assume that the formation and structure of the $[(NH_3)_4Cu_2O_2]^{2+}$-peroxo complex can be affected by the composition and local environment in the zeolite. Indeed, results from in-situ XAS, coupled with WT-EXAFS and Machine Learning (ML) assisted fitting methods show that the structure of the $[(NH_3)_4Cu_2O_2]^{2+}$-peroxo complex and NH_3-SCR performance are affected by the Si/Al ratio and Al distribution in the zeolite.[73]

The Cu–K-edge XANES spectra for the $[(NH_3)_4Cu_2O_2]^{2+}$-peroxo complex in for three Cu-CHA catalysts (1.51 wt% Cu, Si/Al = 5, 2.64 wt% Cu, Si/Al = 15, and 1.71 wt% Cu, Si/Al = 29) are shown in Figure 5a. We note that after the formation of the the $[(NH_3)_4Cu_2O_2]^{2+}$-peroxo complex at 200 °C, the fraction of Cu^{I} (pie charts Figure 5a) for Si/Al = 29 is higher than that for Si/

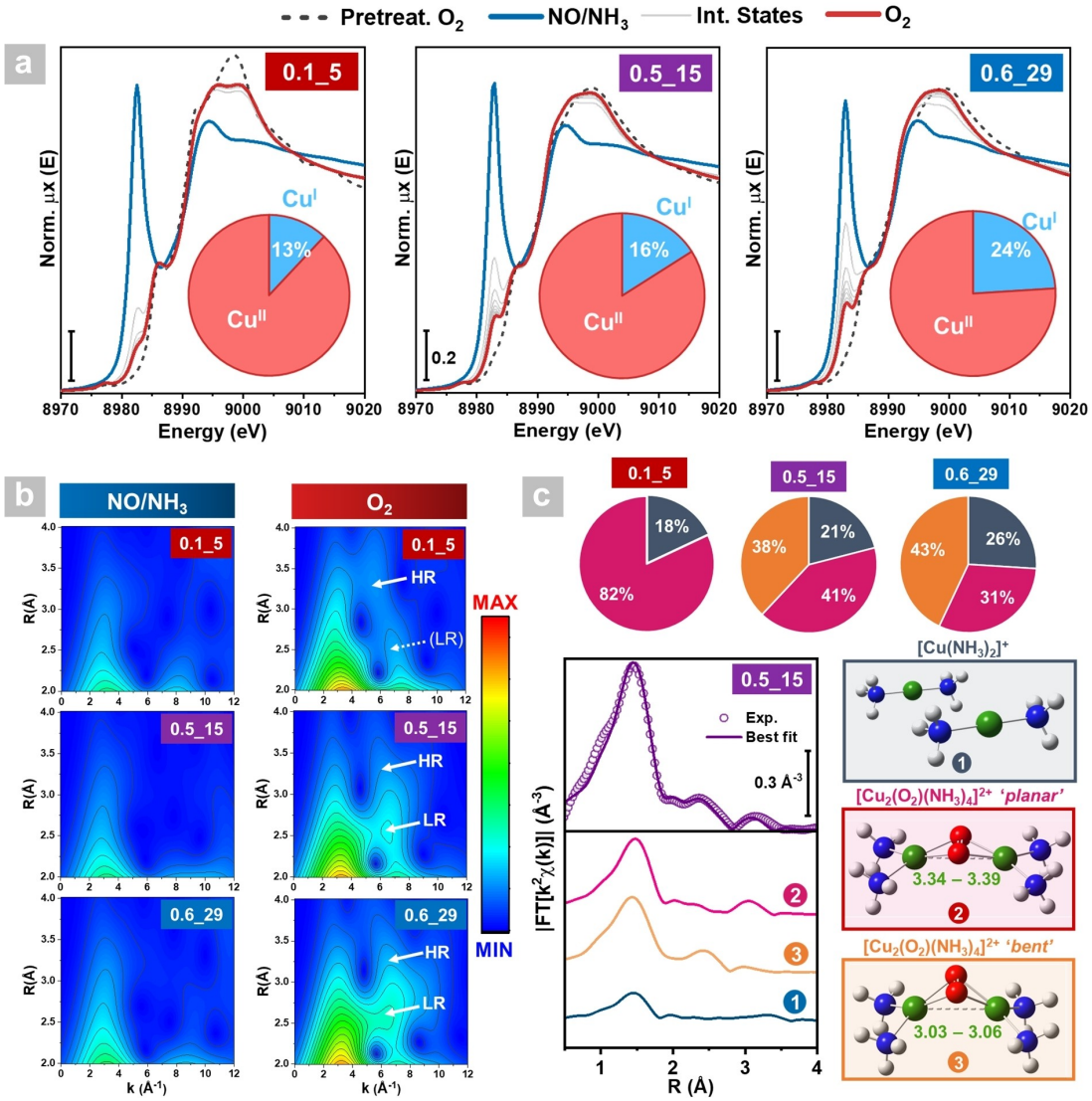

Figure 5. (a) In situ Cu K-edge XANES for Cu-CHA catalysts after pre-treatment, reduction, and oxidation: (a) 1.51 wt% Cu, Cu/Al = 0.11, Si/Al = 5 ("0.1_5"), (b) 2.64 wt% Cu, Cu/Al = 0.47, Si/Al = 15 ("0.5_15") and (c) 1.71 wt% Cu, Cu/Al = 0.56, Si/Al = 29 ("0.6_29"). Pie charts illustrate Cu^{I}/Cu^{II} percentages evaluated by XANES Linear Combination Fit (LCF) at the end of the oxidation step. (b). EXAFS-WT maps after reduction (left) and oxidation (right), magnified in the 2–4 Å range. (c) Example of ML-assisted EXAFS fitting for 1.51 wt% Cu / Si/Al = 5 with molecular models of the employed structural components and their percentages determined for the three catalysts after the oxidation step, illustrated by the pie charts. Summary of results presented in Ref. [73].

Al = 5, even though the Cu densities in these catalysts are comparable. The data by Paolucci et al.[30] follow the same trend. The turn over frequency increases with decreasing Cu^{I} fraction indicating that a more efficient oxidation of $(NH_3)_2Cu^{I}$ by O_2 activation is beneficial for the low temperature NH_3-SCR performance.[73]

A more detailed structural analysis based on the WT-EXAFS maps obtained after oxidation in O_2 (Figure 5b) reveals the presence of dicopper(II) complexes in all catalysts. Additionally, two distinct Cu–Cu interatomic distances can be identified (LR and HR labels with white arrows in Figure 5b), indicating a bimodal distribution of the Cu–Cu distance along the R direction, which suggests the presence of two different structures of the dicopper(II) complexes. A novel Machine Learning-assisted EXAFS analysis, accounting for the presence of $(NH_3)_2Cu^{I}$ and a bimodal distribution of Cu–Cu distances in the $[(NH_3)_4Cu_2O_2]^{2+}$-peroxo complex, confirmed the presence of two different configurations corresponding to a 'bent' and a 'planar' configuration.[73] At Si/Al = 5, the $[(NH_3)_4Cu_2O_2]^{2+}$-peroxo complex adopts the planar configuration, characterized by a Cu–Cu separation of 3.34–3.39 Å (structure 2 in Figure 5c). At the higher Si/Al ratios, about 50–60% of the $[(NH_3)_4Cu_2O_2]^{2+}$-peroxo complexes adopts the bent configuration, with a Cu–Cu distance of 3.03-3.06 Å (structure 3 in Figure 5c). These results clearly show an effect of the Si/Al ratio of the Cu-CHA material on the structure of the $[(NH_3)_4Cu_2O_2]^{2+}$-peroxo complex.

The bent and planar configurations are possibly important for the reactivity of the $[(NH_3)_4Cu_2O_2]^{2+}$-peroxo complex. Steady-state kinetics and operando XAS measurements[74] show

that, at low Al content (Si/Al >12), the NH_3-SCR activity increases with the Al content, which is ascribed to easier paring of the $(NH_3)_2Cu^I$ complexes. In catalysts with higher Al content, the reduction of the $[(NH_3)_4Cu_2O_2]^{2+}$-peroxo complex becomes more difficult, possibly due to the presence of more than one co-caged NH_4^+. This would be an explanation for the well known inhibition of the NH_3-SCR rate by ammonia.[75,76] This behavior parallels the presence of the bent and planar configurations of the $[(NH_3)_4Cu_2O_2]^{2+}$-peroxo complex, and it could therefore be speculated that the more difficult reduction is related to the change in structure of the $[(NH_3)_4Cu_2O_2]^{2+}$-peroxo complex from the bent to the planar configuration.

5. Reactivity of the $[(NH_3)_4Cu_2O_2]^{2+}$-Peroxo Complex

The NH_3-SCR reaction cycle consists of alternating oxidation and reduction steps, with the oxidation of the linear $(NH_3)_2Cu^I$ complex to form the $[(NH_3)_4Cu_2O_2]^{2+}$-peroxo complex as the oxidation step. The NH_3-SCR cycle is then closed by a reduction of the $[(NH_3)_4Cu_2O_2]^{2+}$-peroxo complex to the linear $(NH_3)_2Cu^I$ complex via reactions with NO and NH_3. Consequently, the low-temperature NH_3-SCR activity of Cu-CHA catalysts depends on the reactivity of the $[(NH_3)_4Cu_2O_2]^{2+}$-peroxo complex towards NH_3 and NO.

Experimental confirmation of the reduction of the $[(NH_3)_4Cu_2O_2]^{2+}$-peroxo complex in a mixture of NO and NH_3 to the linear $(NH_3)_2Cu^I$ is provided by in-situ XAS. Exposure of the $[(NH_3)_4Cu_2O_2]^{2+}$-peroxo complex to a 1:1 mixture of NO and NH_3 at 200 °C results in a complete conversion to $(NH_3)_2Cu^I$.[24] In the WT analysis of the corresponding EXAFS spectra, the sub-lobe around $k=7$ Å^{-1} is absent after reduction, indicating that the reduction is accompanied by the cleavage of the Cu–Cu core in the $[(NH_3)_4Cu_2O_2]^{2+}$-peroxo complex. The reduction is most efficient when NO and NH_3 are present together, though some reduction of Cu also occurs in the presence of NO or NH_3 alone, albeit to a lesser extent.[21,24] Interestingly, the sub-lobe at $k=7$ Å^{-1} also disappears when the $[(NH_3)_4Cu_2O_2]^{2+}$-peroxo complex is exposed to NO or NH_3 separately at 200 °C, which implies that in both cases the Cu–Cu core of the $[(NH_3)_4Cu_2O_2]^{2+}$-peroxo complex is cleaved, or at least, the bonding of the Cu-ions to the peroxo-group is modified to result in a less ordered Cu–Cu configuration.

The reaction of NH_3 with $[(NH_3)_4Cu_2O_2]^{2+}$-peroxo complex in the absence of NO leads to a mixed-valence state, containing a Cu^I fraction of ca. 58% total Cu, as estimated by XANES Linear Combination Fit analysis, similar to the partial reduction by NH_3 of Cu-nitrate.[15] This indicates that reaction of NH_3 with the $[(NH_3)_4Cu_2O_2]^{2+}$-peroxo complex does not result in the complete reduction of the Cu to the linear $(NH_3)_2Cu^I$ complex, supporting the conclusion that NO is essential for the reduction of the $[(NH_3)_4Cu_2O_2]^{2+}$-peroxo complex. According to EXAFS, the Cu species formed are most likely the linear $(NH_3)_2Cu^I$ complex, and a $[Cu^{II}(NH_3)_3(X)]^+$ species, similar to a $[Cu^{II}(NH_3)_3(OH)]^+$ species.[44,57]

Upon reaction with NO, the XANES region of the spectra show predominantly a Cu^I state, characterized by the absence of a pre-edge peak at ~ 8977 eV, stemming from the 1 s→3d transition in d^9 Cu^{II} centres, and a prominent 1 s→4p peak at ~8982 eV, indicative for the formation of the linear $(NH_3)_2Cu^I$ complex.[24] This indicates an effective reduction of the $[(NH_3)_4Cu_2O_2]^{2+}$-peroxo complex and means that the reduction of the $[(NH_3)_4Cu_2O_2]^{2+}$-peroxo complex essentially takes place through a reaction with NO, and that at least a part of the NH_3 ligands are retained. A reduction of Cu by NO has been proposed earlier, under the formation of NO^+ or NO_2[77] as intermediates. In more recently proposed reaction mechanisms, the reaction of NO leads to the formation of H_2NNO and HONO intermediates.[9,10,76] We note, that the reduction of the $[(NH_3)_4Cu_2O_2]^{2+}$-peroxo complex corresponds to exposure of the $(NH_3)_2Cu^I$ complex to O_2 and NO at 200 °C in consecutive steps; if the $(NH_3)_2Cu^I$ complex is exposed to O_2 and NO simultaneously at 200 °C, a Cu-nitrate species is formed, which cannot be reduced by NO.[15] This indicates a higher reactivity of the $[(NH_3)_4Cu_2O_2]^{2+}$-peroxo complex for NO, as compared to Cu-nitrate, and therefore Cu-nitrate is less likely to be an intermediate in the low-tempeature NH_3-SCR reaction.

It has been attempted to exploit the reduction of the $[(NH_3)_4Cu_2O_2]^{2+}$-peroxo complex with NO as a basis to quantify the amount of $[(NH_3)_4Cu_2O_2]^{2+}$-peroxo complexes in a Cu-CHA catalyst via titration methods. Such an approach would provide characterization method to monitor the ability of a Cu-CHA material to form the $[(NH_3)_4Cu_2O_2]^{2+}$-peroxo complex. An easy way to do this would be to prepare the $[(NH_3)_4Cu_2O_2]^{2+}$-peroxo complex via oxidation of the reduced $(NH_3)_2Cu^I$ complex with O_2,[11,27,30] followed by measurement of the NO consumption under controlled conditions. However, the temperature of NO exposure in such measurements causes a change in the measured NO uptake per Cu^{II} ion from 0.77 at 150 °C to 1.04 at 250 °C.[27] This is a problematic result, since the amount of $[(NH_3)_4Cu_2O_2]^{2+}$-peroxo complexes does not depend on the temperature at which the titration is done, and therefore, the measured amount should not depend on the chosen temperature for NO exposure. This means that a measurement of the amount of $[(NH_3)_4Cu_2O_2]^{2+}$-peroxo complexes based on a measured NO consumption may be not conclusive.

Furthermore, the measured NO uptake of about one molecule NO per Cu^{II}[27] does not match the expected uptake that would be required for a complete reduction of the $[(NH_3)_4Cu_2O_2]^{2+}$-peroxo complex to 2 $(NH_3)_2Cu^I$, which would require two NO molecules per Cu^{II}, according to the stoichiometry of the NH_3-SCR reaction cycle. An explanation is that the reaction of NO with the $[(NH_3)_4Cu_2O_2]^{2+}$-peroxo complex stops at some point, due to the lack of NH_3. However, the consumption of 1 NO molecule per Cu has also been measured in a complete reduction of the Cu, resulting in the formation of one N_2 molecule per reduced Cu ion.[16,19,20,32] Nasello et al. propose that this stoichiometry follows from a reaction cycle with the following reduction (RHC) and oxidation (OHC) half cycles:[16]

$$\mathrm{OHC:}\quad 2\,Z-Cu^{I}+0.5\,O_2+H_2O\rightarrow 2\,Z-Cu^{II}OH \tag{6}$$

$$\mathrm{RHC:}\quad 2\,Z-Cu^{II}OH+2\,NO+2\,NH_3\rightarrow 2\,Z-Cu^{I}+2\,N_2+4\,H_2O \tag{7}$$

We note that the sum of these cycles results in the overall stoichiometry of the NH_3-SCR reaction. The reactions explain the experimentally observed one NO molecule consumed and one N_2 molecule formed per reduced Cu ion. The 2 Z-Cu^{II}OH take here the role of the reducible Cu, and should be kinetically equivalent to the $[(NH_3)_4Cu_2O_2]^{2+}$-peroxo complex in such measurements. However, these half cycles are inconsistent with the experimental observation of the formation of a $[(NH_3)_4Cu_2O_2]^{2+}$-peroxo complex. Furthermore, the oxidation step according to Eq. 3 requires some water, but it is known that the oxidation of Cu^{I} and NH_3-SCR also takes place in a dry atmosphere in the range 150–300 °C.[10,11,15,78] Therefore, it is not likely that H_2O acts as a reactant in the NH_3-SCR reaction. In fact, H_2O seems to inhibit the NH_3-SCR reaction in this temperature range.[78]

To account for the formation of the $[(NH_3)_4Cu_2O_2]^{2+}$-peroxo complex, we can adjust Eqs. 3 and 4 as follows. First, we observe that the O_2 bridge in the $[(NH_3)_4Cu_2O_2]^{2+}$-peroxo complex contains 2 O^- ions, given that the Cu ions are Cu^{II} ions, yielding the overall 2+ charge on the complex as required by charge neutrality for the zeolite system. This negative charge would then correspond to that of the OH^- ions in the two Z-Cu^{II}OH groups in Eqs. 3 and 4. Therefore, Eqs. 3 and 4 could be reformulated as follows (omitting the NH_3 ligands for clarity):

$$\mathrm{OHC:}\quad 2\,Z-Cu^{I}+O_2\rightarrow Z_2-Cu^{II}_2O_2 \tag{8}$$

$$\mathrm{RHC:}\quad Z_2-Cu^{II}_2O_2+2\,NO+2\,NH_3\rightarrow 2\,Z-Cu^{I}+2\,N_2+3\,H_2O+0.5\,O_2 \tag{9}$$

Eq. 5 then represents the oxidation of a pair of $(NH_3)_2Cu^{I}$ to the $[(NH_3)_4Cu_2O_2]^{2+}$-peroxo complex. No water is needed for the oxidation, in agreement with the observation that the oxidation and formation of the $[(NH_3)_4Cu_2O_2]^{2+}$-peroxo complex also occurs in dry environments.[24] Adding Eqs. 8 and 9 results in the correct stoichiometry for NH_3-SCR (see Eq. 1). However, an oxygen atom is formed, which then needs to react somewhere in the catalytic cycle, without further consumption of NO, to keep the NO:Cu ratio to 1:1. Following this reasoning, some O_2 should be formed during the reduction, though there exists no experimental evidence for such a O_2 formation. The fundamental difficulty of the reaction stoichiometry as discussed above originates from the fact that the oxygen atoms react separately in the NH_3-SCR reaction, thus at some point leaving a single O atom. If that O atom reacts with the reactants NO, the NO:Cu ratio becomes 2:1, otherwise we obtain a NO:Cu ratio of 1:1.

The complications and the lack of understanding of the precise reactions of NO with the $[(NH_3)_4Cu_2O_2]^{2+}$-peroxo complex mean that, at present, NO titrations are not yet reliable enough to measure the amount of $[(NH_3)_4Cu_2O_2]^{2+}$-peroxo complexes. An alternative way to measure the amount of reducible Cu^{II} is by CO oxidation at 200 °C.[26,79–81] This circumvents the complications of possible side reactions with NH_3 present in the catalysts. The amount of formed CO_2 measures the amount of reducible Cu^{II} species. Since the reaction requires multinuclear Cu-complexes, this method provides a reliable measurement of the amount of $[(NH_3)_4Cu_2O_2]^{2+}$-peroxo complexes in Cu-CHA catalysts.

6. First-Principles Reaction Kinetics for NH_3-SCR

The knowledge about the formation and reactivity of the $[(NH_3)_4Cu_2O_2]^{2+}$-peroxo complex forms the basis for NH_3-SCR reaction cycles guided by first-principles (DFT) calculations, using the mean-field approach.[9,10] According to the current understanding, the only reaction step capable of oxidation of the $(NH_3)_2Cu^{I}$ complexes at around 200 °C is the oxidation by O_2, resulting in the $[(NH_3)_4Cu_2O_2]^{2+}$-peroxo complex. Therefore, the NH_3-SCR activity is determined by the reactivity of the $[(NH_3)_4Cu_2O_2]^{2+}$-peroxo complex with NO and NH_3. By taking into account the entropy effects, the free energy profiles of the reaction cycle and activation barriers ($\Delta G^{\ddagger}$) are calculated, which correspond to the rate constants for the individual reaction steps, according to the transition state theory.[82,83] The advantage of such models is that the level of detail allows for relating observed kinetic effects to precise structures and reaction steps in the reaction cycle. The challenge, however, is to validate such detailed models with experimental observations, and even if the model agrees with experimental kinetics, other pathways may still be possible.

Figure 6 shows two possible reaction cycles, based on DFT calculations, for the entire NH_3-SCR reaction.[10] The cycles are based on a reaction of the $[(NH_3)_4Cu_2O_2]^{2+}$-peroxo complex with NO. In cycle I, the reaction of the NO molecule takes place on one of the Cu ions in the $[(NH_3)_4Cu_2O_2]^{2+}$-peroxo complex; in cycle II, the NO reacts with the bridging peroxo-group. This results in different reaction intermediates, even though the overall reaction paths are similar. The reaction with NO leads to HONO and H_2NNO intermediates, that are released from the Cu complexes to react to the products N_2 and H_2O on the acidic Brønsted sites in the zeolite.[9] This model implies, that the overall NH_3-SCR reaction requires both a Cu ion for the initial reaction steps, and a Brønsted acid site to form the N_2 and H_2O reaction by decomposition of the HONO and H_2NNO intermediates. In both cycles, the reaction of the $[(NH_3)_4Cu_2O_2]^{2+}$-peroxo complex with NH_3 results in an extra NH_3 ligand, rendering the complex inactive for NH_3-SCR. The latter reaction accounts for the known inhibition of the NH_3-SCR reaction by NH_3[75,76] in this model.

A further analysis of the kinetics of the reaction cycles in Figure 6 indicates that cycle I is about 10 times faster than cycle II below 250 °C,[10] which suggests that cycle I gives the better description of the NH_3-SCR reaction at low temperatures. A comparison of the calculated reaction orders for NO, NH_3, and O_2, and the calculated activation energies based on these reaction cycles is given in Table 1.[10] The calculated activation energies of 0.75 eV (72 kJ/mol) for cycle I, with the inclusion of the NH_3 inhibition step (step 15), agrees well with the experimentally determined values.[15–17,28,75,77] Likewise, the corre-

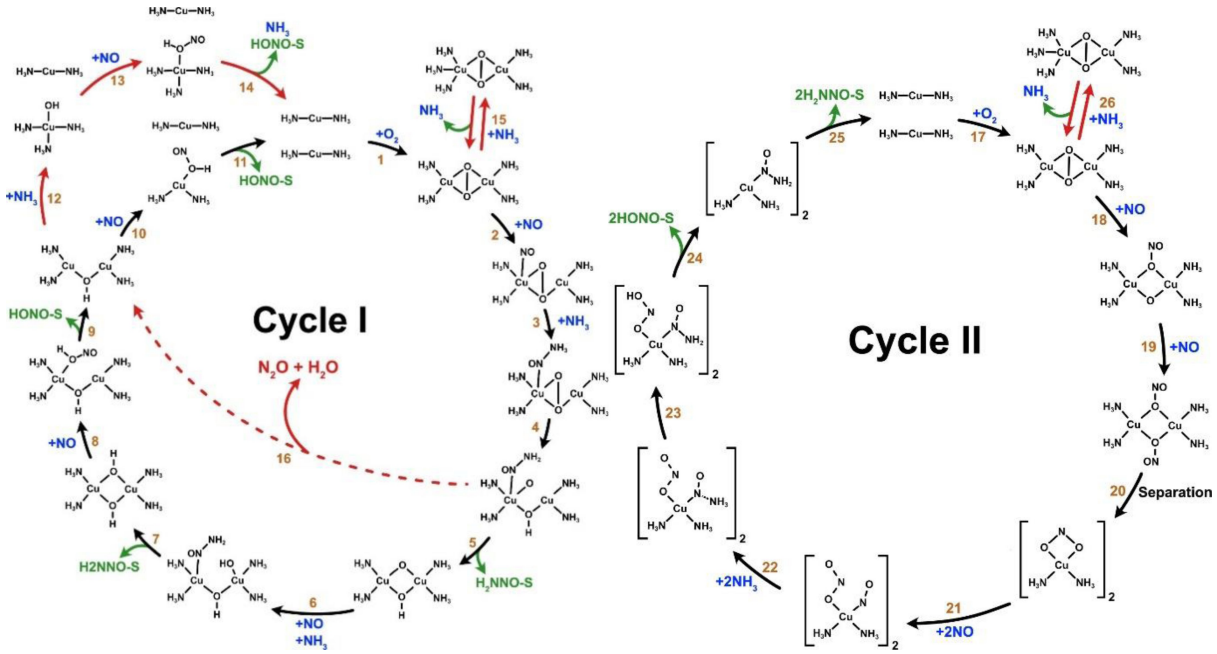

Figure 6. Proposed reaction cycles for the NH_3-SCR reaction over Cu-CHA catalysts, based on the reactivity of the $[(NH_3)_4Cu_2O_2]^{2+}$-peroxo complex. Cycle I: reaction of NO on a Cu-center. Cycle II: reaction of NO on the oxygen bridge in the $[(NH_3)_4Cu_2O_2]^{2+}$-peroxo complex. Reproduced from Ref. [10]. Copyright © 2021 Y. Feng et al. Published by American Chemical Society. This publication is licensed under CC-BY 4.0.

Table 1. Experimental and Calculated Apparent Activation Energy and Reaction Orders for NH_3-SCR over Cu-CHA (1.6 wt% Cu, Si/Al = 6.7). From Ref. [10].

	exp.	cycle I	cycle I w/o NH_3 inhibition (step 15)	cycle II	cycle II w/o NH_3 inhibition (step 26)
apparent E_{act}	0.62/0.89	0.75	0.31	1.06	0.05
order NH_3	−0.23	−0.22	0.05	−0.76	0.00
order NO	0.73	0.95	0.92	1.00	0.99
order O_2	0.25	0.23	0.34	0.15	0.58

sponding reaction orders agree well with the experimental values as well, though the experimentally determined reaction order for NO of about 0.7 is slightly lower than the calculated value of 0.95..[10,75] It is noted that omission of the NH_3-inhibition step in cycle I results in an activation energy of 0.31 eV (30 kJ/mol), indicating that the experimentally observed activation energy is largely determined by the NH_3-inhibition step, even though that reaction step is a side reaction to the main NH_3-SCR reaction cycle. The calculated activation energies based on cycle II clearly deviate from the experimental results, which is consistent with the conclusion that this reaction cycle does not significantly contribute to the overall reaction rate below 250 °C.[10]

We note that the reaction cycles I and II do not include a dissociation of the Cu-pair upon interaction of the $[(NH_3)_4Cu_2O_2]^{2+}$-peroxo complex with NH_3, as has been determined experimentally[24] (see Sect. 5), but merely state that the $[(NH_3)_4Cu_2O_2]^{2+}$-peroxo complex becomes inactive for NH_3-SCR upon reaction with NH_3. A dissociation of the Cu-pair would also result in an inactive intermediate, and therefore, the two descriptions will result in similar kinetic behavior, as discussed in a simplified version of the kinetic model.[84]

To determine the critical reaction steps for the NH_3-SCR rate, a degree of rate control analysis has been applied to reaction cycle I, for the temperature range 100–250 °C; the results are shown in Figure 7. According to this analysis, the reaction of NO with the $[(NH_3)_4Cu_2O_2]^{2+}$-peroxo complex (step 2) is rate determining below 150 °C, as the availability of $[(NH_3)_4Cu_2O_2]^{2+}$-peroxo complex is determined by the NH_3-inhibition equilibrium (step 15). At higher temperatures, a reaction step of NO with a $[(NH_3)_4Cu_2OH_2]^{2+}$-complex (step 8) and the first reaction step with NH_3 (step 3) start to contribute to the overall reaction rate; at 250 °C, step 2, 3, and 8 contribute in about equal amounts to the overall rate. As steps 3 and 8 are considered to be a part of the reduction half cycle, this result corroborates the observation that the overall reaction rate for NH_3-SCR in the temperature range 200–250 °C is determined by both the oxidation and reduction steps, without a clear single rate determining step.[16,17,20,32] In fact, step 8 corresponds to the reduction of 2 Z-CuOH groups, as mentioned in Eq. 6.[16] The corresponding fractions of Cu^{I} and Cu^{II} derived from this model agree well with experimental observation.[10,17] The detailed knowledge of the influence of the individual reaction steps also allows for construction of simpler kinetic models, that preserve

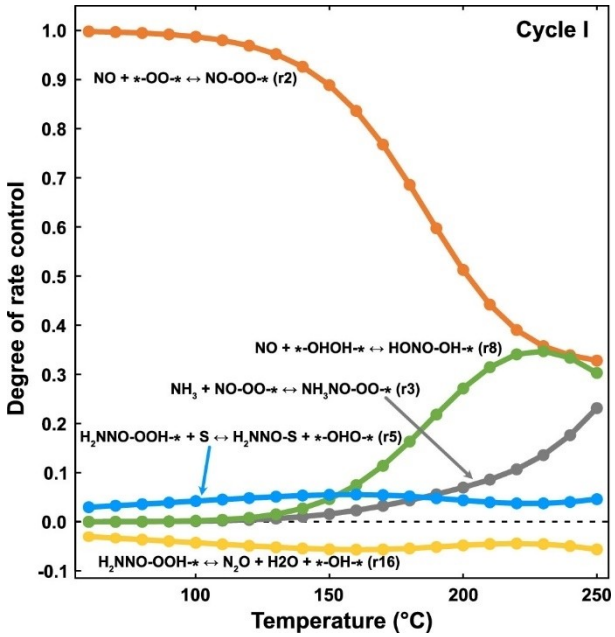

Figure 7. Degree of rate control analysis for cycle I. Reproduced from Ref. [10]. Copyright © 2021 Y. Feng et al. Published by American Chemical Society. This publication is licensed under CC-BY 4.0.

the relation to the underlying chemistry and result in a good approximation of the reaction rates.[10,84]

Other interesting aspects of the reaction cycles in Figure 6 are the different roles of NH_3, and the formation of N_2O. Four different roles for NH_3, namely (1) ligand NH_3, bound to the Cu ions, (2) inhibiting NH_3, adsorbing on the $[(NH_3)_4Cu_2O_2]^{2+}$-peroxo complex (3) reactant NH_3, and (4) NH_3 as NH_4^+ on the Brønsted acid sites are outlined.[10] In order to construct precise kinetic models for NH_3-SCR, these roles must be accounted for, implying that models based on a single total NH_3-coverage or NH_3-content must be expected to have limited validity. In the models, the reactant NH_3 is the NH_3 in the gas phase, entered via the partial pressure.

Cycle I includes a reaction path for the formation of N_2O. The formation of N_2O has been associated to a decomposition of ammonium nitrate in the pores of the CHA zeolite.[6,85] However, the decomposition of ammonium nitrate has an activation barrier of about 1.5-1.8 eV,[86–88] and more favorable energy landscapes are found for N_2O formation as a side reaction.[86] Cycle I proposes that the formation of N_2O occurs in parallel to the first H_2NNO intermediate in the NH_3-SCR cycle (steps 5 and 16 in cycle I), without the formation of an ammonium nitrate species. The energy barrier for this step is 0.40 eV,[10] significantly lower than the barrier for the decomposition of ammonium nitrate. In contrast to the much faster NH_3-SCR reaction, the N_2O formation does not require a Brønsted acid site to proceed.[10] This means that, according to this model, the selectivity to N_2O is determined by the availability of Brønsted acid sites, and catalysts with a high Cu loading, not leaving sufficient Brønsted acid sites for the decomposition of the H_2NNO and HONO intermediates in the NH_3-SCR cycle, are therefore expected to show a higher selectivity for N_2O. Such a trend has been observed experimentally,[89] though a quantitative agreement still needs to be verified. Furthermore, because N_2O formation does not occur in reaction cycle II, this is a further indication that the NH_3-SCR reaction follows cycle I in the temperature range 150–300 °C.[10]

It should be noted that reaction cycle I assumes the presence of two Cu^I in a CHA-cage. However, the presence of Cu-pairs could limit the reaction, in particular at low Cu content.[16,30,32] Assuming the presence of a pair overestimates the rate for the NH_3-SCR reaction. This seems to be corroborated by the fact that the calculated turnover frequency for the NH_3-SCR reaction of about 0.1 s^{-1}, based on cycle I[10] is clearly higher than the TOF for the reduction of the Cu^{II} – this presumably is the $[(NH_3)_4Cu_2O_2]^{2+}$-peroxo complex – reported by Daya et al.[27] Furthermore, it is assumed that a Brønsted acid site for the decomposition of the H_2NNO and HONO intermediates is readily available. Particularly at higher Cu loadings, this is not necessarily true. According to cycle I, a lack of Brønsted sites would result in a lower NH_3-SCR rate. In fact, this might be the reason for the lower experimental value for the reaction order of NO, as compared to the calculated value based on cycle I. Finally, the NO consumption in cycle I (and cycle II) clearly is 2 per Cu ion, which does not match the value observed in the measurement of the reduction half cycle as explained in Sect. 5. However, because the NH_3-SCR reaction rate is largely determined by the oxidation half cycle,[10] in particular below 200 °C, a change in the stoichiometry of the reduction does not necessarily result in a change of the rate of the entire NH_3-SCR cycle.

7. Deactivation of Cu-CHA Catalysts by SO_2

A drawback of Cu-CHA catalysts for NH_3-SCR is their sensitivity towards SO_2. Prolonged exposure to SO_2 can cause severe deactivation in the low-temperature range (below 350 °C). In practice, this means that application of Cu-CHA zeolites in exhaust systems requires the use of ultra-low sulfur diesel (ULSD), which contain less than 10 (Europe) or 15 (US) ppm sulfur on weight basis, to minimize the partial pressure of SO_2 in the exhaust gas. Generally, a Cu-CHA catalyst loses most of the activity below 350 °C upon exposure to SO_2, which to a large extent can be recovered by heating to 500–550 °C (see Figure 8, left panel). However, the deactivation occurs rapidly upon SO_2 exposure, but stabilizes after the loss of about 90% of the original activity (see Figure 8, right panel); the catalysts never loose their low-temperature activity completely. Regeneration by heating then reinstates most of the lost activity, but, typically 10–30% of the original activity cannot be recovered this way.[90,91]

The impact of SO_2 on the NH_3-SCR activity implies that SO_2 interacts with the Cu-CHA catalyst under NH_3-SCR conditions. Figure 9 shows how SO_2 affects the in-situ Cu–K edge XANES spectra of different framework bound and NH_3-solvated Cu^I and Cu^{II} -species in a Cu-CHA catalyst with 3.2 wt% Cu and Si/Al ratio of 6.7.[11] While the spectra for Cu^I and framework bound

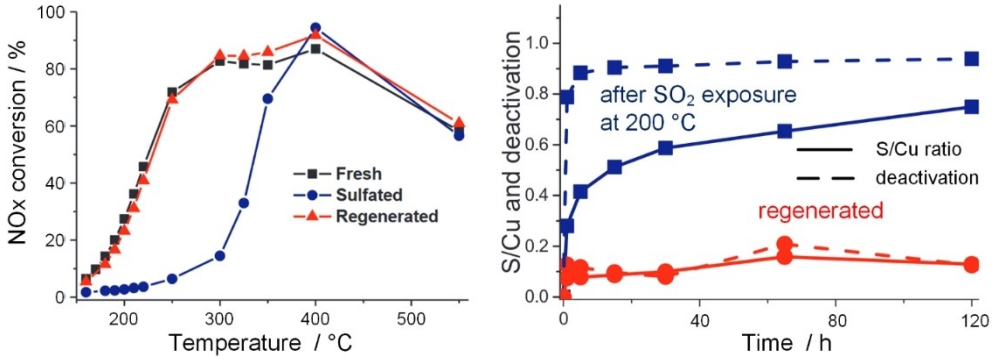

Figure 8. Left panel: Measured NOx conversions over Cu-CHA catalyst (2.8 wt% Cu, Si/Al = 14.7) in the fresh state, after exposure to SO_2 (100 ppm SO_2, 10% O_2, bal. N_2 at 550 °C), and after regeneration (heating in 500 ppm NO/533 ppm NH_3/5% H_2O/10% O_2/bal. N_2 at 550 °C for 4.5 h). From Ref. [90]. Right panel: measured S/Cu ratio and deactivation with time of exposure to 50 ppm SO_2 at 200 °C. From Ref. [91].

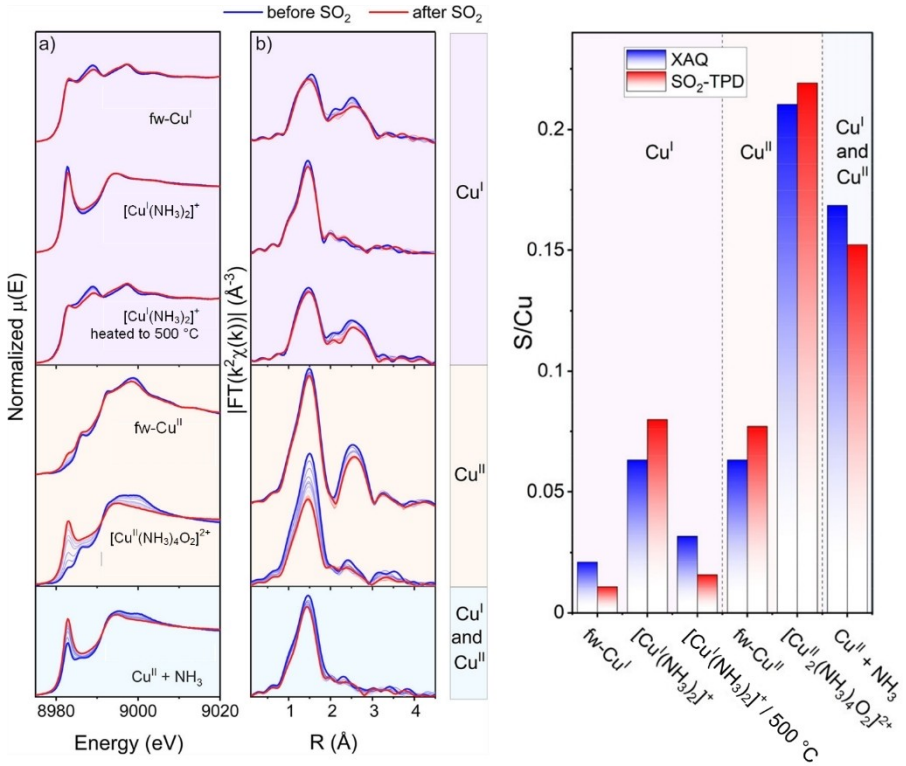

Figure 9. Left panel: In-situ Cu–K edge XANES and corresponding FT EXAFS upon exposure of Cu-CHA (3.2 wt% Cu, Si/Al = 6.7) to 400 ppm SO_2 for framework-bound Cu^I, $(NH_3)_2Cu^I$, $(NH_3)_2Cu^I$ heated to 500 °C, framework-bound Cu^{II}, the $[(NH_3)_4Cu_2O_2]^{2+}$-peroxo complex, and framework-bound Cu^{II} exposed to NH_3. Right panel: Measured sulfur uptake by X-ray Adsorbate Quantification and SO_2-TPD from the same Cu-species. From Ref. [11].

Cu^{II} only change slightly upon SO_2 exposure at 200 °C, the spectra for the $[(NH_3)_4Cu_2O_2]^{2+}$-peroxo complex and Cu^{II} in the presence of NH_3 show significant changes, indicating that SO_2 reacts with Cu^{II} in the presence of NH_3. In fact, the XANES spectra for the $[(NH_3)_4Cu_2O_2]^{2+}$-peroxo complex indicate a reaction with SO_2, in which the $[(NH_3)_4Cu_2O_2]^{2+}$-peroxo complex breaks up and the Cu is partially reduced to the linear $(NH_3)_2Cu^I$ complex. This formation of $(NH_3)_2Cu^I$ is further corroborated by the lower 1st shell coordination around R = 1.5 Å, as such a reaction implies a reduction in coordination from 4 to 2. The total uptake of SO_2, as determined by X-ray Adsorbate Quantification (XAQ)[92] and temperature programmed desorption of SO_2 (SO_2-TPD), is also clearly enhanced for Cu^{II} species in the presence of NH_3 (Figure 9 right panel). These results indicate that the interaction of SO_2 with the Cu in the Cu-CHA catalysts preferably proceeds via a reaction with the $[(NH_3)_4Cu_2O_2]^{2+}$-peroxo complex. The observation that poisoning by SO_2 is enhanced in the presence of an NH_3-SCR feed gas (NH_3/NO/O_2/H_2O), as compared to poisoning by SO_2 in the presence of O_2 and H_2O only,[93] provides further indirect evidence for the $[(NH_3)_4Cu_2O_2]^{2+}$-peroxo complex as a critical component for deactivation by SO_2.

The fact that SO_2 reacts with the $[(NH_3)_4Cu_2O_2]^{2+}$-peroxo complex leads to the hypothesis that deactivation by SO_2 is

caused by the formation Cu–S species that are not active for NH_3-SCR. An analysis of the Cu–K edge XANES data indicate the presence of such a sulfated Cu-compound (Figure 10, left panel).[12] The shape of the S K-edge XANES and S Kα XES spectra after interaction of the $[(NH_3)_4Cu_2O_2]^{2+}$-peroxo complex with SO_2 is typical for S^{VI} in tetrahedral coordination, confirming the previous ex-situ results (Figure 10, right panels).[94,95] This means that the Cu–S compound formed in the reaction of the $[(NH_3)_4Cu_2O_2]^{2+}$-peroxo complex with SO_2 is a sulfate-like compound. The formation of a sulfate-like compound is corroborated by the Cu–K-edge XANES and corresponding EXAFS.[11,12] The Cu K-edge XANES features of the Cu–S compound are similar to those of Cu^{2+} in a quasi-square-planar geometry and a coordination to N or O atoms.

A fit of the corresponding EXAFS points to a structure with the two O and two NH_3 ligands situated at slightly different distances (1.94 and 2.09 Å), together with a contribution of S atom, most probably bound to Cu through oxygen ligands, at 2.58 Å, in line with the formation of Cu-sulfate-like species. From the observed formation of Cu^{I} and Cu^{II} compounds in the reaction with SO_2, a two-step reaction was proposed. In the first step a framework-bound Cu^{I} and a sulfur based intermediate, presumably SO_3, are formed, which is then followed by a reaction of that sulfur based intermediate with a second $[(NH_3)_4Cu_2O_2]^{2+}$-peroxo complex to form a Cu-sulfate species, and the $(NH_3)_2Cu^{I}$ complex.[12] Overall, these experimental XAS and XES data provide evidence that $[(NH_3)_4Cu_2O_2]^{2+}$-peroxo complex is the most reactive intermediate in the NH_3-SCR cycle towards SO_2. This reaction then leads to a direct interruption of the NH_3-SCR cycle, and the accumulation of sulfur in the catalyst, resulting in the deactivation.

Another approach to understand the interaction of the $[(NH_3)_4Cu_2O_2]^{2+}$-peroxo complex with SO_2 is to construct a reaction model using density functional theory (DFT). Using this approach, it has been proposed,[13] that SO_2 attaches to the oxygen-bridge in the $[(NH_3)_4Cu_2O_2]^{2+}$-peroxo complex, in agreement with the spectroscopic data,[11,12] however, arriving at a different mechanism for the deactivation of the Cu-CHA. In the scheme in Ref [13], the Cu^{I} species does not form immediately in a reaction with SO_2, but would still require a further reaction step with NO, in contrast to the observation in XAS, that Cu^{I} species appear in the absence of NO.[12] Eventually ammonium sulfate is formed, via a sulfuric acid intermediate, and Cu-sulfate like species. The presence of ammonium sulfate then influences the ability of the $(NH_3)_2Cu^{I}$ complexes to form the Cu pairs and formation of the $[(NH_3)_4Cu_2O_2]^{2+}$-peroxo complexes. In fact, it is shown that the presence of a single ammonium-sulfate unit in a zeolite cage actually stabilizes the formation of Cu-pairs, and that the destabilization of Cu-pairs first occurs when two ammonium sulfate units are present in the cage.[13] This scenario would imply that Cu-CHA catalysts can tolerate SO_2 below a certain critical uptake of sulfur. This, however, contradicts the observation that the deactivation is fast in the initial phases of SO_2 exposure, and that the observed activity is decreased by 90 % at S/Cu ratios well below 1 (see Figure 8, right panel).[91]

Because the $[(NH_3)_4Cu_2O_2]^{2+}$-peroxo complex is solvated by NH_3-ligands, it cannot directly be related to a specific site in the zeolite, such as the Z_2-Cu^{II} site in the *6mr*-rings, or a Z-Cu^{II}OH site, which are the most common locations for a Cu^{II} ion in the zeolite. Consequently, the effect of SO_2 on the low-temperature NH_3-SCR activity is not directly determined by the location of the Cu ions in the zeolite. Moreover, the Z_2-Cu^{II} and Z-Cu^{II}OH sites represent framework-bound Cu^{II} species, which are not very reactive towards SO_2 (see Figure 9).[11,12] This suggests that, in principle, the deactivation by SO_2 is not very dependent on the framework locations of the Cu ions in the zeolite. Nevertheless, a number of studies rationalize experimental observations in terms of the reactivity of Z_2-Cu^{II} and Z-Cu^{II}OH sites towards SO_2.[96–101] Experimental evidence for a different interaction of SO_2 with these Cu species is provided by FTIR of

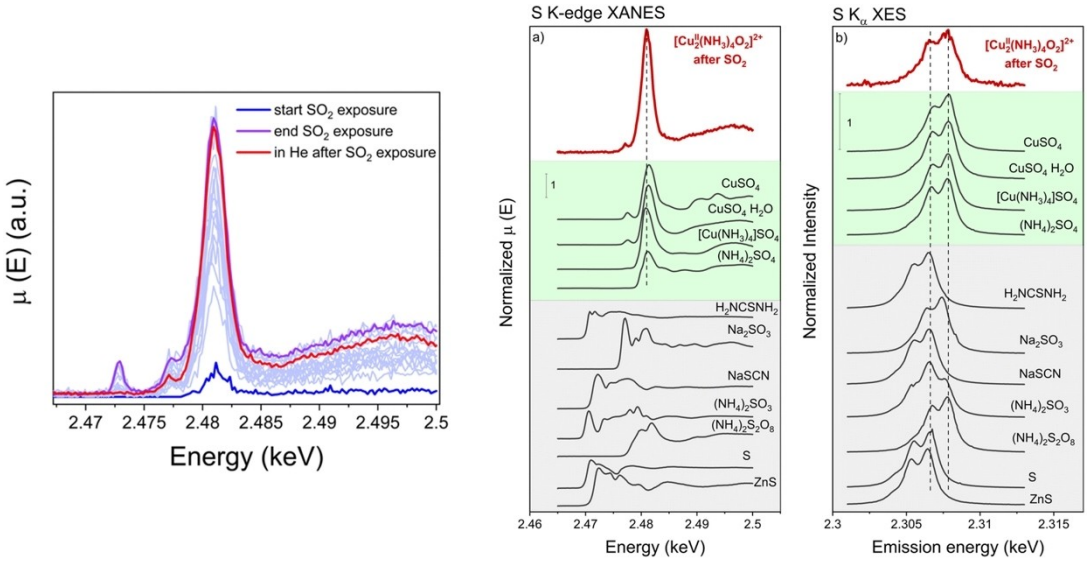

Figure 10. Left panel: In-situ XANES at the S–K edge upon exposure of the $[(NH_3)_4Cu_2O_2]^{2+}$-peroxo complex to 100 ppm SO_2 at 200 °C. Right panel: Comparison of the S–K edge in XANES and XES S Kα emission lines of the $[(NH_3)_4Cu_2O_2]^{2+}$-peroxo complex exposed to SO_2 with reference compounds. Reproduced from Ref. [12] with permission from the Royal Society of Chemistry.

antisymmetric [TO_4] vibrations of the zeolite framework in the 900–1000 cm^{-1} range. The strong electrostatic interaction of the framework-bound Z_2-Cu^{II} and Z-Cu^{II}OH perturbs the antisymmetric [TO_4] vibration of the zeolite framework. When Z_2-Cu^{II} and Z-Cu^{II}OH become solvated by NH_3, the perturbation is weakened, resulting in negative bands at 900 and 950 cm^{-1} in the FTIR spectrum, corresponding to the solvation of the Z_2-Cu^{II} and Z-Cu^{II}OH, respectively.[96,97,102,103] Figure 11 shows the effect of SO_2 on the solvation process for the Z_2-Cu^{II} and Z-Cu^{II}OH species, by monitoring the FTIR bands at 900 and 950 cm^{-1} during exposure to NH_3 in the absence and presence of SO_2. When SO_2 is present during the NH_3 exposure, the measured intensity ratio I_{950}/I_{900} is lower than that measured in the absence of SO_2 (left and middle panels in Figure 11). This indicates that the effect of SO_2 is different for the Z-Cu^{II}OH and Z_2-Cu^{II} sites.

A different interaction for Z_2-Cu^{II} and Z-Cu^{II}OH is further supported by temperature-programmed desorption of SO_2 (SO_2-TPD). In a Cu-CHA catalyst with Si/Al = 30, a larger fraction of the SO_2 desorbs at around 600 °C, as compared to a Cu-CHA catalyst with Si/Al = 6, as shown in the right panel in Figure 11. Since a catalyst with a high Si/Al ratio is expected to contain more Z-Cu^{II}OH,[17] this indicates a stronger interaction of SO_2 with a catalyst that contains more Z-Cu^{II}OH. The total amount of SO_2 observed in these TPD measurements are 563 μmol/g for the 3.58 wt% Cu-CHA (Si/Al = 6) catalyst, and 204 μmol/g for the 1.20 wt% Cu-CHA (Si/Al = 30) catalyst;[97] these values correspond to S/Cu ratios of 1.01 and 1.08, respectively. This suggests that the total uptake of SO_2 is limited and determined by the amount of Cu in the zeolite, in full agreement with the formation of a Cu-sulfate-like compound, as determined from XAS measurements.[12] However, the two distinct features in SO_2-TPD also indicate that different Cu-sulfate-like species are formed, dependent on the Cu content and Si/Al ratio of the zeolite. The formation of excessive amounts of ammonium sulfate can then be excluded, as this would lead to significantly higher amounts of SO_2 in the TPD measurement.

To reconcile the observed differences in the interaction of SO_2 with Z-Cu^{II}OH and Z_2-Cu^{II} with the observation that the interaction of SO_2 takes place via an interaction with the $[(NH_3)_4Cu_2O_2]^{2+}$-peroxo complex, the formation of the $[(NH_3)_4Cu_2O_2]^{2+}$-peroxo complex from Z-Cu^{II}OH and Z_2-Cu^{II} must be considered. In principle, the formation of $[(NH_3)_4Cu_2O_2]^{2+}$-peroxo complex depends on the mobility and pair formation of the $(NH_3)_2Cu^{I}$ complexes. Experiments indicate, that both Z_2-Cu^{II} and Z-Cu^{II}OH sites are reduced and mobilized as $(NH_3)_2Cu^{I}$ complexes upon reduction in a NO/NH_3 mixture at 200 °C.[56,104] The question remains whether and how the mobility and reactivity of $(NH_3)_2Cu^{I}$ complexes are affected by the Al content, and the corresponding negative charge density, in the zeolite. Furthermore, Z-Cu^{II}OH sites can be mobilized as $[(NH_3)_3Cu^{II}$-$(OH)]^{+}$ in the presence of NH_3, which can diffuse between the zeolite cages in the CHA structure. In contrast, inter-cage diffusion is not possible for $[(NH_3)_4Cu^{II}]^{2+}$ formed from Z_2-Cu^{II}, due to the electrostatic tethering of the divalent complex.[26,80] This different behavior of Z-Cu^{II}OH and Z_2-Cu^{II} provides a way how the corresponding reduction and pair formation of $(NH_3)_2Cu^{I}$ complexes can be different. The Cu^{I}-pairs formed from the more mobile Z-Cu^{II}OH may be located further away from their Al anchor points in the zeolite structure.

In conclusion, it is certain that the interaction of SO_2 with Cu-CHA catalyst for NH_3-SCR proceeds via the $[(NH_3)_4Cu_2O_2]^{2+}$-peroxo complex. That reaction leads to a partial reduction of the Cu to Cu^{I}, and the oxidation of SO_2 to a Cu-sulfate-like species, while the formation of ammonium sulfate seems less likely. The S atom in the Cu-sulfate-like species is in an S^{VI} oxidation state, which is bound to the Cu-ions via an oxygen atom, as expected for a Cu-sulfate-like species. The precise identification of all compounds involved in the uptake of sulfur, and the mechanism for the observed deactivation, however, have not been solved yet. Because a small amount of SO_2, corresponding to S/Cu ratios of 0.4-1 causes a loss of 80–90% of the low-temperature activity for NH_3-SCR, the most probable mechanism for the deactivation by SO_2 is a disturbance of the NH_3-SCR reaction cycle via the interaction of SO_2 with the $[(NH_3)_4Cu_2O_2]^{2+}$-peroxo complex.

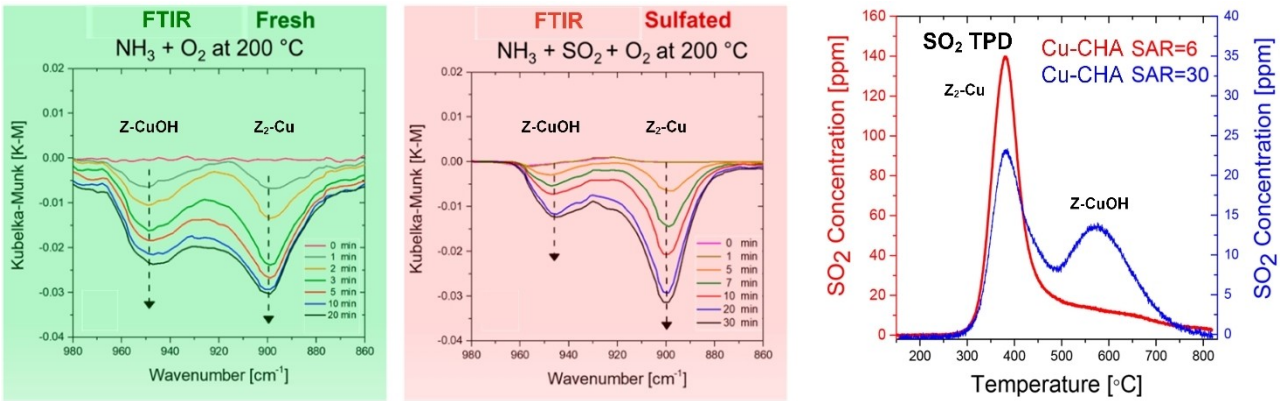

Figure 11. FTIR of the TO_4-framework vibrations in Cu-CHA (Si/Al ratio 30, 1.2 wt% Cu) upon exposure to $NH_3 + O_2$ at 200 °C (left panel) or $NH_3 + SO_2 + O_2$ at 200 °C (middle panel), and SO_2-TPD from Cu-CHA with Si/Al ratio 6 and 30 (right panel). Reprinted with permission from Ref. [97] Copyright © 2018, American Chemical Society.

8. Final Remarks

The basis of the current understanding of the Cu-CHA catalysts for NH_3-SCR in the temperature range 150–300 °C is that the first step is the adsorption of molecular oxygen on a pair of mobile $(NH_3)_2Cu^I$ complexes.[18,30,34] The key role of this step provides insight in how catalyst properties, such as the Cu content, the Al content and Al distribution can influence the reaction. The chemical properties $[(NH_3)_4Cu_2O_2]^{2+}$-peroxo complex that is formed determine to a high degree the catalytic behavior of Cu-CHA catalysts in NH_3-SCR. The NH_3-SCR activity is governed by the reactivity of the $[(NH_3)_4Cu_2O_2]^{2+}$-peroxo complex towards NO (see Sect. 5),[24] and the application of this idea has led to a successful kinetic model of the NH_3-SCR reaction based on the formulation of a reaction pathway at the molecular level (see Sect. 6).[9,10] The negative reaction order in NH_3 for NH_3-SCR (NH_3-posioning) results from a reaction of NH_3 with $[(NH_3)_4Cu_2O_2]^{2+}$-peroxo complex[10] (see Sect. 6), which leads to a dissociation of the Cu-pair in the $[(NH_3)_4Cu_2O_2]^{2+}$-peroxo complex (see Sect. 5).[24] Finally, the deactivation by SO_2 is a consequence of a reaction of SO_2 with the $[(NH_3)_4Cu_2O_2]^{2+}$-peroxo complex, under the formation of Cu-sulfate-like compounds (see Sect. 7).[11,12]

There are also some remaining questions regarding impact of the chemistry of the $[(NH_3)_4Cu_2O_2]^{2+}$-peroxo complex on the performance of Cu-CHA catalysts for NH_3-SCR. First, the 'bent' and 'planar' configurations of the $[(NH_3)_4Cu_2O_2]^{2+}$-peroxo complex seems to result in a different rate of the reduction half cycle (see Sect. 4). It remains unclear if this is really the case, how it works, and how the configuration of the $[(NH_3)_4Cu_2O_2]^{2+}$-peroxo complex is affected by the structure of the zeolite, Si/Al ratio and Cu content. Second, the reaction cycles based on the formation of the $[(NH_3)_4Cu_2O_2]^{2+}$-peroxo complex imply a 2:1 NO:Cu ratio in the reduction half cycle of the NH_3-SCR reaction,[9,10] whereas separate measurements of the oxidation and reduction half-cycles indicate a 1:1 NO:Cu ratio.[16,19,20,32] This could mean that the reaction cycles proposed so far are not entirely correct, even though they result in correct reaction orders, and activation energies. Third, the deactivation by SO_2 results from a reaction of SO_2 with the $[(NH_3)_4Cu_2O_2]^{2+}$-peroxo complex, under the formation of a Cu-sulfate-like species, the sulfur atom in the S^{VI} oxidation state. However, this resulting Cu-sulfate-like species has not been identified exactly yet.[12] Furthermore, a DFT based model for deactivation by SO_2 suggests that the deactivation is due to accumulation of some ammonium sulfate in the zeolite cages,[13] which is not consistent with the observed deactivation behavior.[91]

Other aspects of the chemistry of the $[(NH_3)_4Cu_2O_2]^{2+}$-peroxo complex that have not yet been considered are the thermal stability of the $[(NH_3)_4Cu_2O_2]^{2+}$-peroxo complex, and the possible impact of water on the reactions with the $[(NH_3)_4Cu_2O_2]^{2+}$-peroxo complex. With respect to the thermal stability, we can expect that the NH_3 ligands are lost at higher temperatures, similar to the decomposition of the linear $(NH_3)_2Cu^I$ complex, which occurs around 250–300 °C.[57,105] The well-known decrease in NOx conversion around 300 °C ("seagull" effect) is often related to the decomposition of the $(NH_3)_2Cu^I$ complexes, resulting in the loss of their mobility,[18,58] such that the formation of the $[(NH_3)_4Cu_2O_2]^{2+}$-peroxo complex becomes more difficult. However, it can be expected that the thermal stability of the $[(NH_3)_4Cu_2O_2]^{2+}$-peroxo complex plays a similar role. In addition, the reactivity of the oxygen bridge may change at higher temperatures, and this may affect the rate of the NH_3-SCR reaction via a change of the reduction half cycle.

The impact of water on the chemistry of the $[(NH_3)_4Cu_2O_2]^{2+}$-peroxo complex has so far not been considered. It is known that the presence of water affects the kinetics of the NH_3-SCR reaction. For example, the activation energy of the reduction half cycle is 20 kJ/mol lower in the presence of water,[106] which may due to a change in the chemistry of the $[(NH_3)_4Cu_2O_2]^{2+}$-peroxo complex. Moreover, below 250 °C, Cu^{II} becomes solvated by water molecules,[107,108] introducing another type of mobility in the system. In view of the recent developments for ammonia-powered and hydrogen-powered internal combustion engines (HICE), which are possible technologies to reduce greenhouse gas emissions in the transportation sector, the impact of water on the performance of NH_3-SCR catalysts will become an important issue. In a hydrogen-powered combustion engine, the water content in the exhaust will typically be well above 10%, dependent on the air/fuel ratio, and becomes 34% at the stoichiometric air/fuel ratio.[109,110] Hydrogen-powered engines produce on the order of 500–5000 ppm NOx, primarily due to the higher temperature in the combustion, as compared to conventional combustion engines.[110,111] NOx emissions from hydrogen-powered combustion engines can be effectively reduced by conventional Cu-CHA catalysts.[110] Understanding the impact of a high concentration of water will therefore be important for a successful implementation of Cu-CHA catalysts for NOx abatement in combustion engines based on non-fossil fuels.

Acknowledgements

Support from the European Union's Horizon 2020 research and innovation programme under the Marie Sklodowska-Curie grant agreement No. 955839 (CHASS) is gratefully acknowledged. HG acknowledges financial support from the Swedish Energy Agency (47110-1 and 52689-1). GB and EB acknowledge support from the Project CH4.0 under the MUR program "Dipartimenti di Eccellenza 2023–2027" (CUP: D13C22003520001).

Conflict of Interests

The authors declare no conflict of interest.

[1] J. H. Kwak, R. G. Tonkyn, D. H. Kim, J. Szanyi, C. H. F. Peden, *J. Catal.* **2010**, *275*, 187–190.
[2] D. W. Fickel, E. D'Addio, J. A. Lauterbach, R. F. Lobo, *Appl. Catal. B* **2011**, *102*, 441–448.
[3] U. Deka, A. Juhin, E. a Eilertsen, H. Emerich, M. a Green, S. T. Korhonen, B. M. Weckhuysen, A. M. Beale, *J. Phys. Chem. C* **2012**, *116*, 4809–4818.
[4] D. W. Fickel, R. F. Lobo, *J. Phys. Chem. C* **2010**, *114*, 1633–1640.

[5] J. H. Kwak, D. Tran, S. D. Burton, J. Szanyi, J. H. Lee, C. H. F. Peden, *J. Catal.* **2012**, *287*, 203–209.
[6] H.-Y. Chen, Z. Wei, M. Kollar, F. Gao, Y. Wang, J. Szanyi, C. H. F. Peden, *J. Catal.* **2015**, *329*, 490–498.
[7] O. US EPA, "GHG Emission Factors Hub," can be found under https://www.epa.gov/climateleadership/ghg-emission-factors-hub, **2015**.
[8] S. Elkaee, S. Y. Kim, A. D. Phule, Md. W. Uz Zaman, S. G. Lee, G. Park, J. Hwan Yang, *J. Environ. Chem. Eng.* **2023**, *11*, 111131.
[9] L. Chen, T. V. W. Janssens, P. Vennestrøm, J. Jansson, M. Skoglundh, H. Grönbeck, *ACS Catal.* **2020**, *10*, 5646–5656.
[10] Y. Feng, X. Wang, T. V. W. Janssens, P. N. R. Vennestrøm, J. Jansson, M. Skoglundh, H. Grönbeck, *ACS Catal.* **2021**, *11*, 14395–14407.
[11] A. Yu. Molokova, E. Borfecchia, A. Martini, I. A. Pankin, C. Atzori, O. Mathon, S. Bordiga, F. Wen, P. N. R. Vennestrøm, G. Berlier, T. V. W. Janssens, K. A. Lomachenko, *JACS Au* **2022**, *2*, 787–792.
[12] A. Y. Molokova, R. K. Abasabadi, E. Borfecchia, O. Mathon, S. Bordiga, F. Wen, G. Berlier, T. V. W. Janssens, K. A. Lomachenko, *Chem. Sci.* **2023**, *14*, 11521–11531.
[13] J. D. Bjerregaard, M. Votsmeier, H. Grönbeck, *J. Catal.* **2023**, *417*, 497–506.
[14] C. Paolucci, A. A. Verma, S. A. Bates, V. F. Kispersky, J. T. Miller, R. Gounder, W. N. Delgass, F. H. Ribeiro, W. F. Schneider, *Angew. Chem. Int. Ed.* **2014**, *53*, 11828–11833.
[15] T. V. W. Janssens, H. Falsig, L. F. Lundegaard, P. N. R. Vennestrøm, S. B. Rasmussen, P. G. Moses, F. Giordanino, E. Borfecchia, K. A. Lomachenko, C. Lamberti, S. Bordiga, A. Godiksen, S. Mossin, P. Beato, *ACS Catal.* **2015**, *5*, 2832–2845.
[16] N. D. Nasello, N. Usberti, U. Iacobone, F. Gramigni, W. Hu, S. Liu, I. Nova, X. Gao, E. Tronconi, *ACS Catal.* **2023**, *13*, 2723–2734.
[17] C. Paolucci, A. A. Parekh, I. Khurana, J. R. Di Iorio, H. Li, J. D. Albarracin Caballero, A. J. Shih, T. Anggara, W. N. Delgass, J. T. Miller, F. H. Ribeiro, R. Gounder, W. F. Schneider, *J. Am. Chem. Soc.* **2016**, *138*, 6028–6048.
[18] F. Gao, D. Mei, Y. Wang, J. J. Szanyi, C. H. F. Peden, *J. Am. Chem. Soc.* **2017**, *139*, 4935–4942.
[19] W. Hu, T. Selleri, F. Gramigni, E. Fenes, K. R. Rout, S. Liu, I. Nova, D. Chen, X. Gao, E. Tronconi, *Angew. Chem. Int. Ed.* **2021**, *60*, 7197–7204.
[20] D. J. Deka, R. Daya, A. Ladshaw, S. Y. Joshi, W. P. Partridge, *Chem. Eng. J.* **2022**, *435*, 134219.
[21] D. J. Deka, R. Daya, S. Y. Joshi, W. P. Partridge, *Appl. Catal. Gen.* **2022**, *640*, 118656.
[22] A. R. Fahami, I. Nova, Enrico. Tronconi, *Catal. Today* **2017**, *297*, 10–16.
[23] P. S. Hammershøi, C. Negri, G. Berlier, S. Bordiga, P. Beato, T. V. W. Janssens, *Catal. Sci. Technol.* **2019**, *9*, 2608–2619.
[24] C. Negri, T. Selleri, E. Borfecchia, A. Martini, K. A. Lomachenko, T. V. W. Janssens, M. Cutini, S. Bordiga, G. Berlier, *J. Am. Chem. Soc.* **2020**, *142*, 15884–15896.
[25] C. Negri, E. Borfecchia, A. Martini, G. Deplano, K. A. Lomachenko, T. V. W. Janssens, G. Berlier, S. Bordiga, *Res. Chem. Intermed.* **2021**, *47*, 357–375.
[26] W. Hu, F. Gramigni, N. D. Nasello, N. Usberti, U. Iacobone, S. Liu, I. Nova, X. Gao, E. Tronconi, *ACS Catal.* **2022**, 5263–5274.
[27] R. Daya, D. Trandal, U. Menon, D. J. Deka, W. P. Partridge, S. Y. Joshi, *ACS Catal.* **2022**, *12*, 6418–6433.
[28] F. Gao, E. D. Walter, M. Kollar, Y. Wang, J. Szanyi, C. H. F. F. Peden, *J. Catal.* **2014**, *319*, 1–14.
[29] A. M. Beale, F. Gao, I. Lezcano-Gonzalez, C. H. F. Peden, J. Szanyi, *Chem. Soc. Rev.* **2015**, *44*, 7371–7405.
[30] C. Paolucci, I. Khurana, A. A. Parekh, S. Li, A. J. Shih, H. Li, J. R. Di Iorio, J. D. Albarracin-Caballero, A. Yezerets, J. T. Miller, W. N. Delgass, F. H. Ribeiro, W. F. Schneider, R. Gounder, *Science* **2017**, *357*, 898–903.
[31] F. Gao, C. H. F. Peden, *Catalysts* **2018**, *8*, 140.
[32] F. Gramigni, N. D. Nasello, N. Usberti, U. Iacobone, T. Selleri, W. Hu, S. Liu, X. Gao, I. Nova, E. Tronconi, *ACS Catal.* **2021**, 4821–4831.
[33] H. Falsig, P. N. R. Vennestrøm, P. G. Moses, T. V. W. Janssens, *Top. Catal.* **2016**, *59*, 861–865.
[34] L. Chen, H. Falsig, T. V. W. Janssens, H. Grönbeck, *J. Catal.* **2018**, *358*, 179–186.
[35] A. Wijerathne, A. Sawyer, R. Daya, C. Paolucci, *JACS Au* **2024**, DOI 10.1021/jacsau.3c00632.
[36] J. S. Woertink, P. J. Smeets, M. H. Groothaert, M. A. Vance, B. F. Sels, R. A. Schoonheydt, E. I. Solomon, *Proc. Nat. Acad. Sci.* **2009**, *106*, 18908–18913.
[37] M.-L. Tsai, R. G. Hadt, P. Vanelderen, B. F. Sels, R. A. Schoonheydt, E. I. Solomon, *J. Am. Chem. Soc.* **2014**, *136*, 3522–3529.
[38] P. Vanelderen, B. E. R. Snyder, M.-L. Tsai, R. G. Hadt, J. Vancauwenbergh, O. Coussens, R. A. Schoonheydt, B. F. Sels, E. I. Solomon, *J. Am. Chem. Soc.* **2015**, *137*, 6383–6392.
[39] Y. Feng, T. V. W. Janssens, P. N. R. Vennestrøm, J. Jansson, M. Skoglundh, H. Grönbeck, *J. Phys. Chem. C* **2024**, *128*, 6689–6701.
[40] G. Deplano, A. Martini, M. Signorile, E. Borfecchia, V. Crocellà, S. Svelle, S. Bordiga, *Angew. Chem. Int. Ed.* **2021**, *60*, 25891–25896.
[41] M. Signorile, E. Borfecchia, S. Bordiga, G. Berlier, *Chem. Sci.* **2022**, *13*, 10238–10250.
[42] C. W. Andersen, E. Borfecchia, M. Bremholm, M. R. V. Jørgensen, P. N. R. Vennestrøm, C. Lamberti, L. F. Lundegaard, B. B. Iversen, *Angew. Chem. Int. Ed.* **2017**, *56*, 10367–10372.
[43] A. M. Beale, I. Lezcano-Gonzalez, W. A. Slawinksi, D. S. Wragg, *Chem. Commun.* **2016**, *52*, 6170–6173.
[44] C. Negri, E. Borfecchia, M. Cutini, K. A. Lomachenko, T. V. W. Janssens, G. Berlier, S. Bordiga, *ChemCatChem* **2019**, *11*, 3828–3838.
[45] F. Giordanino, E. Borfecchia, K. A. Lomachenko, A. Lazzarini, G. Agostini, E. Gallo, A. V. Soldatov, P. Beato, S. Bordiga, C. Lamberti, *J. Phys. Chem. Lett.* **2014**, *5*, 1552–1559.
[46] R. Millan, P. Cnudde, V. Van Speybroeck, M. Boronat, *JACS Au* **2021**, *1*, 1778–1787.
[47] C. Paolucci, J. R. Di Iorio, W. F. Schneider, R. Gounder, *Acc. Chem. Res.* **2020**, *53*, 1881–1892.
[48] L. Chen, J. Jansson, M. Skoglundh, H. Grönbeck, *J. Phys. Chem. C* **2016**, *120*, 29182–29189.
[49] R. Millan, E. Bello-Jurado, M. Moliner, M. Boronat, R. Gomez-Bombarelli, *ACS Cent. Sci.* **2023**, *9*, 2044–2056.
[50] S. Shwan, M. Skoglundh, L. F. Lundegaard, R. R. Tiruvalam, T. V. W. Janssens, A. Carlsson, P. N. R. Vennestrøm, *ACS Catal.* **2015**, *5*, 16–19.
[51] A. Y. Stakheev, D. A. Bokarev, A. I. Mytareva, T. V. W. Janssens, P. N. R. Vennestrøm, *Top. Catal.* **2017**, *60*, 255–259.
[52] P. N. R. Vennestrøm, L. F. Lundegaard, C. Tyrsted, D. A. Bokarev, A. I. Mytareva, G. N. Baeva, A. Y. Stakheev, T. V. W. Janssens, *Top. Catal.* **2019**, *62*, 100–107.
[53] C. B. Jones, *J. Catal.* **2020**, *10*.
[54] X. Wang, L. Chen, P. N. R. Vennestrøm, T. V. W. Janssens, J. Jansson, H. Grönbeck, M. Skoglundh, *ChemCatChem* **2021**, *13*, 2577–2582.
[55] M. Moreno-González, B. Hueso, M. Boronat, T. Blasco, A. Corma, *J. Phys. Chem. Lett.* **2015**, *6*, 1011–1017.
[56] K. A. Lomachenko, E. Borfecchia, C. Negri, G. Berlier, C. Lamberti, P. Beato, H. Falsig, S. Bordiga, *J. Am. Chem. Soc.* **2016**, *138*, 12025–12028.
[57] E. Borfecchia, C. Negri, K. A. Lomachenko, C. Lamberti, T. V. W. Janssens, G. Berlier, *React. Chem. Eng.* **2019**, *4*, 1067–1080.
[58] A. R. Fahami, T. Günter, D. E. Doronkin, M. Casapu, D. Zengel, T. H. Vuong, M. Simon, F. Breher, A. V. Kucherov, A. Brückner, J.-D. Grunwaldt, *React. Chem. Eng.* **2019**, *4*, 1000–1018.
[59] L. Chen, T. V. W. Janssens, H. Grönbeck, *Phys. Chem. Chem. Phys.* **2019**, *21*, 10923–10930.
[60] A. Oda, H. Shionoya, Y. Hotta, T. Takewaki, K. Sawabe, A. Satsuma, *ACS Catal.* **2020**, *10*, 12333–12339.
[61] M. Metz, E. I. Solomon, *J. Am. Chem. Soc.* **2001**, *123*, 4938–4950.
[62] J. P. Perdew, K. Burke, M. Ernzerhof, *Phys. Rev. Lett.* **1996**, *77*, 3865–3868.
[63] H. Rydberg, B. I. Lundqvist, D. C. Langreth, M. Dion, *Phys. Rev. B* **2000**, *62*, 6997–7006.
[64] H. Rydberg, M. Dion, N. Jacobson, E. Schröder, P. Hyldgaard, S. I. Simak, D. C. Langreth, B. I. Lundqvist, *Phys. Rev. Lett.* **2003**, *91*, 126402.
[65] M. Dion, H. Rydberg, E. Schröder, D. C. Langreth, B. I. Lundqvist, *Phys. Rev. Lett.* **2004**, *92*, 246401.
[66] T. Thonhauser, V. R. Cooper, S. Li, A. Puzder, P. Hyldgaard, D. C. Langreth, *Phys. Rev. B* **2007**, *76*, 125112.
[67] K. Berland, P. Hyldgaard, *Phys. Rev. B* **2014**, *89*, 035412.
[68] J. Wellendorff, K. T. Lundgaard, A. Møgelhøj, V. Petzold, D. D. Landis, J. K. Nørskov, T. Bligaard, K. W. Jacobsen, *Phys. Rev. B: Condens. Matter Mater. Phys.* **2012**, *85*, 32–34.
[69] P. L. Holland, W. B. Tolman, *Coord. Chem. Rev.* **1999**, *190–192*, 855–869.
[70] D. K. Pappas, E. Borfecchia, M. Dyballa, I. A. Pankin, K. A. Lomachenko, A. Martini, M. Signorile, S. Teketel, B. Arstad, G. Berlier, C. Lamberti, S. Bordiga, U. Olsbye, K. P. Lillerud, S. Svelle, P. Beato, *J. Am. Chem. Soc.* **2017**, *139*, 14961–14975.
[71] C. Negri, M. Signorile, N. G. Porcaro, E. Borfecchia, G. Berlier, T. V. W. Janssens, S. Bordiga, *Appl. Catal. Gen.* **2019**, *578*, 1–9.
[72] J. A. Halfen, S. Mahapatra, E. C. Wilkinson, S. Kaderli, V. G. Young, L. Que, A. D. Zuberbühler, W. B. Tolman, *Science* **1996**, *271*, 1397–1400.

[73] A. Martini, C. Negri, L. Bugarin, G. Deplano, R. K. Abasabadi, K. A. Lomachenko, T. V. W. Janssens, S. Bordiga, G. Berlier, E. Borfecchia, *J. Phys. Chem. Lett.* **2022**, *13*, 6164–6170.
[74] S. H. Krishna, A. Goswami, Y. Wang, C. B. Jones, D. P. Dean, J. T. Miller, W. F. Schneider, R. Gounder, *Nat. Catal.* **2023**, *6*, 276–285.
[75] S. A. Bates, A. A. Verma, C. Paolucci, A. A. Parekh, T. Anggara, A. Yezerets, W. F. Schneider, J. T. Miller, W. N. Delgass, F. H. Ribeiro, *J. Catal.* **2014**, *312*, 87–97.
[76] Y. Zhang, Y. Peng, K. Li, S. Liu, J. Chen, J. Li, F. Gao, C. H. F. Peden, *ACS Catal.* **2019**, *9*, 6137–6145.
[77] F. Gao, J. H. Kwak, J. Szanyi, C. H. F. Peden, *Top. Catal.* **2013**, *56*, 1441–1459.
[78] L. Ma, Z. Li, H. Zhao, T. Zhang, N. Yan, J. Li, *ACS EST Eng.* **2022**, *2*, 1684–1696.
[79] H. Li, C. Paolucci, I. Khurana, L. N. Wilcox, F. Göltl, J. D. Albarracin-Caballero, A. J. Shih, F. H. Ribeiro, R. Gounder, W. F. Schneider, *Chem. Sci.* **2019**, *10*, 2373–2384.
[80] R. Villamaina, U. Iacobone, I. Nova, M. P. Ruggeri, J. Collier, D. Thompsett, E. Tronconi, *ChemCatChem* **2020**, *12*, 3843–3848.
[81] P. D. Costa, B. Modén, G. D. Meitzner, D. K. Lee, E. Iglesia, *Phys. Chem. Chem. Phys.* **2002**, *4*, 4590–4601.
[82] H. Eyring, *J. Chem. Phys.* **1935**, *3*, 107–115.
[83] I. Chorkendorff, J. W. Niemantsverdriet, in *Concepts Mod. Catal. Kinet.*, John Wiley & Sons, Ltd, **2003**, pp. 79–128.
[84] Y. Feng, D. Creaser, H. Grönbeck, *Top. Catal.* **2023**, *66*, 743–749.
[85] J. Han, A. Wang, G. Isapour, H. Härelind, M. Skoglundh, D. Creaser, L. Olsson, *Ind. Eng. Chem. Res.* **2021**, *60*, 17826–17839.
[86] Y. Feng, T. V. W. Janssens, P. N. R. Vennestrøm, J. Jansson, M. Skoglundh, H. Grönbeck, *J. Phys. Chem. C* **2021**, *125*, 4595–4601.
[87] B. J. Wood, H. Wise, *J. Chem. Phys.* **1955**, *23*, 693–696.
[88] S. Chaturvedi, P. N. Dave, *J. Energ. Mater.* **2013**, *31*, 1–26.
[89] D. Yao, B. Liu, F. Wu, Y. Li, X. Hu, W. Jin, X. Wang, *Ind. Eng. Chem. Res.* **2021**, *60*, 10083–10093.
[90] P. S. Hammershøi, Y. Jangjou, W. S. Epling, A. D. Jensen, T. V. W. Janssens, *Appl. Catal. B* **2018**, *226*, 38–45.
[91] P. S. Hammershøi, A. D. Jensen, T. V. W. Janssens, *Appl. Catal. B* **2018**, *238*, 104–110.
[92] K. A. Lomachenko, A. Yu. Molokova, C. Atzori, O. Mathon, *J. Phys. Chem. C* **2022**, *126*, 5175–5179.
[93] K. Wijayanti, K. Leistner, S. Chand, A. Kumar, K. Kamasamudram, N. W. Currier, A. Yezerets, Louise. Olsson, *Catal. Sci. Technol.* **2016**, *6*, 2565–2579.
[94] Y. Cheng, C. Lambert, D. H. Kim, J. H. Kwak, S. J. Cho, C. H. F. Peden, *Catal. Today* **2010**, *151*, 266–270.
[95] V. Mesilov, S. Dahlin, S. L. Bergman, P. S. Hammershøi, S. Xi, L. J. Pettersson, S. L. Bernasek, *Catal. Sci. Technol.* **2021**, *11*, 5619–5632.
[96] X. Auvray, M. Arvanitidou, Å. Högström, J. Jansson, S. Fouladvand, L. Olsson, *Emiss. Control Sci. Technol.* **2021**, *7*, 232–246.
[97] Y. Jangjou, Q. Do, Y. Gu, L. G. Lim, H. Sun, D. Wang, A. Kumar, J. Li, L. C. Grabow, W. S. Epling, *ACS Catal.* **2018**, *8*, 1325–1337.
[98] A. J. Shih, I. Khurana, H. Li, J. González, A. Kumar, C. Paolucci, T. M. Lardinois, C. B. Jones, J. D. Albarracin Caballero, K. Kamasamudram, A. Yezerets, W. N. Delgass, J. T. Miller, A. L. Villa, W. F. Schneider, R. Gounder, F. H. Ribeiro, *Appl. Catal. Gen.* **2019**, *574*, 122–131.
[99] L. Wei, D. Yao, F. Wu, B. Liu, X. Hu, X. Li, X. Wang, *Ind. Eng. Chem. Res.* **2019**, *58*, 3949–3958.
[100] J. Luo, D. Wang, A. Kumar, J. Li, K. Kamasamudram, N. Currier, A. Yezerets, *Catal. Today* **2016**, *267*, 3–9.
[101] P. S. Hammershøi, P. N. R. Vennestrøm, H. Falsig, A. D. Jensen, T. V. W. Janssens, *Appl. Catal. B* **2018**, *236*, 377–383.
[102] E. Groppo, S. Rojas-Buzo, S. Bordiga, *Chem. Rev.* **2023**, *123*, 12135–12169.
[103] J. H. Kwak, T. Varga, C. H. F. Peden, F. Gao, J. C. Hanson, J. Szanyi, *J. Catal.* **2014**, *314*, 83–93.
[104] R. Villamaina, S. Liu, I. Nova, E. Tronconi, M. P. Ruggeri, J. Collier, A. York, D. Thompsett, *ACS Catal.* **2019**, *9*, 8916–8927.
[105] R. Daya, D. J. Deka, A. Goswami, U. Menon, D. Trandal, W. P. Partridge, S. Y. Joshi, *Appl. Catal. B* **2023**, *328*, 122524.
[106] G. Contaldo, M. Ferri, C. Negri, I. Nova, M. Maestri, E. Tronconi, *ChemCatChem* **2023**, *15*, e202300673.
[107] A. Godiksen, P. N. R. Vennestrøm, S. B. Rasmussen, S. Mossin, *Top. Catal.* **2017**, *60*, 13–29.
[108] A. Godiksen, F. N. Stappen, P. N. R. Vennestrøm, F. Giordanino, S. B. Rasmussen, L. F. Lundegaard, S. Mossin, *J. Phys. Chem. C* **2014**, *118*, 23126–23138.
[109] S. Sterlepper, M. Fischer, J. Claßen, V. Huth, S. Pischinger, *Energies* **2021**, *14*, 8166.
[110] C. Özyalcin, S. Sterlepper, S. Roiser, H. Eichlseder, S. Pischinger, *Appl. Energy* **2024**, *353*, 122045.
[111] J. Kim, *Int. J. Automot. Technol.* **2023**, *24*, 1681–1690.

Manuscript received: February 26, 2024
Revised manuscript received: April 24, 2024
Accepted manuscript online: May 10, 2024
Version of record online: June 24, 2024